polysaccharides

MDPI

Article

Urea Peroxide Embedded in Alginate–Chitosan Compound Coating Material Containing Selenate Altered Redox Potential and Selenium Speciation in Paddy Soil

Xu-Jian Yang [1,2,3,4], Yihang Ouyang [4,†], Kaixia Ma [4,†], Song Bai [1,2,3,*] and Hong Shen [4,*]

[1] Rice Research Institute, Guangdong Academy of Agricultural Sciences, No. 3 Jinying Dong 1 Street, Guangzhou 510640, China; yangxujian@gdaas.cn or zh_yangxujian@scau.edu.cn
[2] Guangdong Key Laboratory of Rice Science and Technology, No. 3 Jinying Dong 1 Street, Guangzhou 510640, China
[3] Guangdong Rice Engineering Laboratory, No. 3 Jinying Dong 1 Street, Guangzhou 510640, China
[4] College of Natural Resources and Environment, South China Agricultural University, No. 483 Wushan Road, Guangzhou 510642, China
* Correspondence: baisong@gdaas.cn (S.B.); hshen@scau.edu.cn (H.S.)
† These authors contributed equally to this work.

Abstract

Low redox potential (*Eh*) leads to low bioavailability and utilization efficiency of several nutrients, including selenium (Se), in paddy soil. Applying oxidants with a slow-release function to maintain soil *Eh* at a sufficiently high level during the key nutrient stage is beneficial to plant-nutrient accumulation. A multi-component coating material consisting of alginate, chitosan, nano-silicon dioxide, carboxymethyl cellulose, and selenate was used to embed urea peroxide to prepare a slow-release fertilizer of oxidative substances in this study. The effects of the components on oxidative substance release and mechanical properties were investigated, and their contribution to altering soil *Eh* and Se speciation was verified by paddy soil assay. The formula containing 20~25 mg g^{-1} alginate, 15 mg g^{-1} chitosan, 30 mg g^{-1} silicon dioxide nanoparticle, 10 mg g^{-1} carboxymethyl cellulose, 0.1 mg g^{-1} sodium selenate, and 150 mg g^{-1} urea peroxide performed the best among treatments. It had satisfactory mechanical properties and an elevated *Eh* with an amplitude of over 100 mV for at least 40 d compared to the soil with a single Se treatment, and increased the contents and proportions of soluble, exchangeable, and a part of iron/manganese-binding Se, especially the hexavalent one, in soil. Notably, selenate not only supplied Se but also contributed to structure reinforcement. The findings provided a slow-release carrier for soil nutrient management, but it still needs to be improved for more coordinated release of Se and oxidative substances.

Keywords: macromolecule matrix; coated fertilizer; compound material; slow release; paddy soil; redox potential (*Eh*); selenium (Se) speciation

Check for updates

Academic Editor: Jaime Lizardi-Mendoza

Received: 11 August 2026
Revised: 20 October 2026
Accepted: 21 October 2026
Published: 5 November 2026

Copyright: © 2026 by the authors. Licensee MDPI, Basel, Switzerland. This article is an open access article distributed under the terms and conditions of the Creative Commons Attribution (CC BY) license.

1. Introduction

Nutrient resources, especially fertilizers, play a role as essential as water, pesticides, and other bioactive compounds in crop yield [1] to meet the rising cereal demand driven by population growth [2]. However, the nutrient-release properties of traditional fertilizers do not always match plant-nutrition demands. Water-soluble nutrients dissolve, diffuse, and deplete rapidly in soil after fertilization [3], which leads to intensive nutrient availability fluctuations, with 30–70% of nutrients lost through leaching or volatilization [4]. Therefore,

good nutrient supply strategies mean lower nutrient input, higher utilization efficiency, better nutrient-release patterns, and less environmental pollution [5–8]. It is labor- and time-consuming to apply traditional fertilizers at low doses several times to meet plant-nutrient demands at different stages of the life cycle. Additionally, there is a proportion of nutrients with low bioavailability in soil due to certain physicochemical factors, i.e., precipitation, specific adsorption, biological immobilization, etc.; thus, soils with high total nutrient contents do not always indicate high fertility.

Selenium (Se) is a beneficial nutrient element for plants and humans that participates in cellular differentiation and functioning, maintaining cellular membrane integrity, reactive oxygen scavenging, and toxin inactivation, alleviating stress resistance and immunity [9–15]. Food Se biofortification, especially in rice, is an optimal means to satisfy human routine Se intake demand since it economically provides Se in biocompatible forms, and rice is an intermediate Se accumulator among cereals [15]. Although cereals and their products provide around 70% of the total dietary Se intake for the public according to estimates, over 72% of arable land in eastern China is in Se-deficient status, and over 75% of rice products cannot satisfy intake requirements [16–20] since the general average level of soil Se is 0.4 mg kg^{-1}, which varies between 0.1 and 2 mg kg^{-1} [21]. Therefore, Se deficiency has become a global public nutrition issue.

Agronomic biofortification, mainly fertilization, is easier and cheaper than genetic biofortification, i.e., crop selection and breeding [22]. External Se input is required for all soils, whatever their Se content, from the perspective of sustainable agriculture because soil Se will be depleted by plant uptake over decades [23]. The valences of Se in soil include +6, +4, 0, and −2 [24]. Although organic Se (mainly amino acids containing Se, i.e., selenomethionine and selenocysteine, and proteins that these Se-containing amino acids participate in constitution) is safer and more efficient for humans, inorganic Se oxyanions (hydroselenite $HSeO_3^-$ and selenate SeO_4^{2-}) are the major available fractions in rhizosphere nutrition, while the organic fraction can be the soil Se reservoir [9,17,25]. Notably, inorganic Se oxyanions at high doses have potential toxicity since the boundary between deficiency and toxicity is narrow. In addition, their utilization efficiency is relatively low, which is more severe for selenite [10,19,26–29]. Li et al. [20] and Yin et al. [30] suggested that fertilizing SeO_4^{2-} in aerobic soil is more efficient for raising Se content in rice grains and more beneficial for photosynthesis promotion than foliar application. Moreover, the heading and boosting stages are the recommended fertilization stages for promoting Se accumulation in brown rice because active growing spikes and filling grains at these stages are the main destination of assimilated Se [12,22,31], but the leaves cover the soil densely and hinder fertilization at those stages. Contrarily, over 80% of inorganic Se fertilized in soil during the vegetative growth stage is sequestered by soil iron or manganese (hydr)oxide colloids or reduced to elemental form [32]; moreover, this process is faster in acidic soils than in neutral and alkaline soils [33]. Subsequently, only 5~30% of soil exogenous Se can be absorbed by plants [34]. Therefore, it is necessary to overcome the above disadvantages using slow/controlled-release fertilizers (S/CRFs) so that the Se fertilized in advance at the vegetable growth stage is continuously supplied to plants in the proper concentration to match nutrient demands [35].

Oxygen in paddy soil is limited in a strongly reductive rhizosphere due to long-term submergence [36]; rice plants attempt to establish the aerobic rhizosphere surroundings by secreting oxygen and other oxidative substances [37,38]. The dominant valence of soil Se is tetravalent under this bulk soil condition, which is easily sequestered by soil colloids [16,32]; i.e., soil Se availability for rice is low during long-term submergence status, and it is accumulated in the root rather than the shoot in rice plants [29,39], which hinders rice Se biofortification. Therefore, raising soil redox potential (*Eh*) is necessary

for more soil SeO_4^{2-} and higher Se accumulation in rice grain [30,40]. However, field water management by draining and irrigation cannot be applied for the long term during the vegetative growth stage because of physiological water demand in the rice life cycle; therefore, other means to alleviate soil redox status are in demand. Urea peroxide is an adduct compound of hydrogen peroxide and urea. It can alleviate rhizosphere redox status and provide nitrogen (N) nutrient efficiently and simultaneously. Moreover, its hydrolytic products are oxygen, carbonates (or carbon dioxide), and ammonium, all of which can be utilized by plants. In addition, supplying N and Se simultaneously can slightly increase grain Se accumulation [41] since ammonium is reported to promote rice Se uptake at the soil–floodwater interface [22]. In any case, controlled-release material should be used to overcome the disadvantages of rapid and uncontrolled oxidative substance release (OSR) after urea peroxide is dissolved, which may lead to acute oxidative damage in roots.

Coating fertilizers are a series of S/CRFs whose core fertilizer is embedded, covered, or encapsulated by hydrophobic release-control polymer materials with semi-permeable properties through chemical cross-linking or physical adhesion [42]. Moreover, it is feasible to mix core fertilizers and polymer coating materials to obtain efficiency-enhancing fertilizers in which nutrients are distributed evenly in the coating material [43]. Since agricultural biomaterials, including chitosan (Chi), alginate (Alg), cellulose, starch, cyclodextrin, etc., have advantages of wide sources, low cost, good biocompatibility and biodegradability, as well as non-toxicity [2,5,44,45], they can be applied as degradable hydrogels after simple chemical or physical modifications [5,46]. The fertilizers made from these hydrogels have higher nutrient utilization efficiency, although the fertilizer input is lower than traditional materials [47]. Alginic acids and alginates extracted from algae are linear polymers of β-D-mannuronic acids and α-L-guluronic acids. Alginate dimers form via ionic bonds between cations (e.g., Ca^{2+}, Ba^{2+}, Fe^{2+}, Al^{3+}) and -OH as well as -COOH groups in guluronate residues [42,48,49]. Calcium alginate (CaAlg) is a potential carrier for nutrients, pesticides, and other agronomic chemicals due to its "egg-box" structure retaining small molecules [5]. Moreover, its coating layer thickness can be easily regulated by Ca^{2+} concentration [42]. However, pure CaAlg is not an ideal CRF material since its coating efficiency is low, and it degrades in soil too fast to regulate the dynamics of embedded nutrient release [6]. Therefore, it is necessary to modify or compound CaAlg with other substances, i.e., apply proper multi-component coating material formulas, for better permeation, release control, and mechanical properties, as well as less nutrient loss during fertilizer preparation [2,50]. Chen et al. [51] designed an alginate-urea-fluroxypyr controlled-release system in which urea bridges Alg and fluroxypyr ingeniously, providing at least 8-week controlled release as a carrier for fertilizer and pesticide. Chi is the degradation product of chitin, which is polymerized from D-aminoglucose and N-acetyl-D-aminoglucose [2,52,53]. A compound membrane forms via cross-linking reactions and electrostatic effects between cationic groups $-NH_3^+$ in Chi and anionic groups $-COO^-$ in Alg [43,47,48]; the cross-linking network, also known as the matrix, reduces pore size remarkably but maintains the coating integrity, which benefits controlled release [54]. Liu et al. [55] developed a compound slow-release fertilizer consisting of a carboxymethyl chitosan resin network and urea aldehyde, which realizes the simultaneous slow release of water and nitrogen nutrients by water-retention technology. Kim et al. [56] created recyclable green plastics with strong mechanical features, whose nanocomposites were made from sodium alginate and Chi nanowhisker, and recommended them as controlled-release materials for urea. Cellulose has good water-retaining capacity, but it is necessary to modify the carbon chains by grafting hydrophilic groups (e.g., hydroxyl or carboxyl), esterification, or etherification to overcome fragility caused by strong hydrogen bonds [57]. Wang et al. [58] introduced a self-assembled CRF whose template is nano-$CaCO_3$, and the coating material consists of carboxymet hylcellulose (CMC)/Alg and Chi.

Similar to Alg, CMC is also able to self-assemble with Chi via -NH_2 and -COOH groups in this case. This fertilizer has nano-sized pores that can adsorb embedded nutrient substances charge-independently by capillary effect; moreover, it exhibits different nutrient-release dynamic properties under different ambient pH conditions. Tan et al. [59] reported a double-layer CRF whose internal coating is polymethylmethacrylate, while the external coating is an alginate hydrogel cross-linked with sulfonated cellulose, which performs satisfactorily in urea release following a first-order kinetic model. Notably, phosphorus-enriched biochar encapsulated by CMC has strong pH buffering capacity, which provides advantageous conditions for stable phosphorus release at low doses [60].

The objective of this study is to attempt to provide a fertilizer product that can alleviate the anoxic rhizosphere of paddy soil, i.e., elevating *Eh*, and alter soil Se fractions, especially increasing the proportion of Se easily utilized by plants, simultaneously establishing suitable soil conditions for Se biofortification. We hypothesized that the coating material consisting of Alg and Chi might be suitable for regulating the release of UP and Se nutrients inside the soil, so that the soil *Eh* and the bioavailable Se concentration were maintained at a satisfactory level for a relatively long period. Therefore, the preparation procedure of multi-component coating materials, whose properties are less fully documented than those of mono-component ones, as well as the mechanical properties and performance on oxidative substances and Se nutrient release of the coated fertilizer granules made with this coating material, were investigated in this study.

2. Materials and Methods

2.1. Materials

2.1.1. Reagents

Calcium chloride ($CaCl_2$, anhydrous substance, CAS 10043-52-4) and carboxymethyl cellulose (CMC, sodium salt, CAS 9004-32-4), whose viscosity was 1000~1500 mPa·s, were purchased from Damao Chemical Reagent Partnership Enterprise Ltd., Tianjin, China. Silicon dioxide nanoparticle (n-SiO_2, CAS 60676-86-0) with a diameter of 50 ± 5 nm was purchased from Macklin Biochemical Technology Co., Ltd., Shanghai, China. The purity of the above three reagents was analytical grade (≥99.5%). Chitosan (Chi, CAS 9012-76-4) (purity ≥ 90%), whose viscosity was 20~500 mPa·s, was purchased from Bozhi Oligo Biotech Co., Ltd., Qingdao, China. Alginate (Alg, sodium salt, CAS 9005-38-3) (purity ≥ 90%) was purchased from Kermel Chemical Reagent Co., Ltd., Tianjin, China. Urea peroxide (UP, CAS 124-43-6) (purity ≥ 96%) was purchased from Sanjie Environmental Protection Technology Co., Ltd., Shijiazhuang, China. Sodium selenate (Na_2SeO_4, CAS 13410-01-0) (purity ≥ 98%) with the trademark "Aike Reagent" was purchased from Boruite Chemical Technology Co., Ltd., Chengdu, China.

2.1.2. Soil

The paddy soil used in this study was collected in Guangzhou, China. Its physical and chemical properties were: texture (International Society of Soil Science system), clay loam; mechanical composition [sand (0.02~2 mm):slit (0.002~0.02 mm):clay (<0.002 mm)], 38.76%:28.45%:32.78%; organic matter, 22.72 g kg^{-1}; pH (natural submergence bulk soil after sufficient equilibrium), 6.60; *Eh* (natural submerging bulk soil after sufficient equilibrium), −29.3 mV; total nitrogen, 0.875 g kg^{-1}; total phosphorus, 1.026 g kg^{-1}; total potassium, 11.27 g kg^{-1}; alkaline- hydrolytic nitrogen, 78.89 mg kg^{-1}; available phosphorus (extracted by pH 8.5 0.5 mol L^{-1} $NaHCO_3$), 74.60 mg kg^{-1}; rapid-available potassium (extracted by pH 7.0 1 mol L^{-1} CH_3COONH_4), 50.16 mg kg^{-1}; total selenium, 396.2 μg kg^{-1}.

2.2. The Preparation Procedure of Fertilizer Granules

Two solutions, named Solution A and Solution B, were used in coating fertilizer preparation. Solution A consisted of $CaCl_2$ and CMC, while Solution B contained Chi, n-SiO_2, Alg, UP, and Na_2SeO_4. The solvent concentrations of Solutions A and B are introduced in Section 2.2 below. Both solutions were prepared by dissolving the corresponding solutes successively into deionized water with sufficient stirring: The $CaCl_2$ was dissolved in deionized water, and then CMC was added to the $CaCl_2$ solution to obtain Solution A. The 1 g L^{-1} Na_2SeO_4 stock solution was added to deionized water at a ratio of 1:1000 (v/v) first when preparing Solution B in the multiple-factor experiment, but it was absent in the single-factor experiment; then, other components in Solution B—Chi, n-SiO_2, Alg, and UP—were dissolved successively. To prevent the formation of pellets in which the moist CMC and Alg encapsulated the dry material in the solution, they were added in several successive portions for complete dissolution. Similarly, UP was also added in several batches to ensure it was distributed uniformly in the final products. For instance, to prepare the formula of 40 mg g^{-1} (the mass proportion of corresponding ingredient in solution, similar hereinafter) $CaCl_2$, 20 mg g^{-1} Alg, 15 mg g^{-1} Chi, 30 mg g^{-1} n-SiO_2, 10 mg g^{-1} CMC, 0.1 mg g^{-1} Na_2SeO_4, and 150 mg g^{-1} UP, 4 g of $CaCl_2$ and 1 g of CMC were dissolved in 95 mL deionized water for Solution A. On the other hand, 5 mL of 1 g L^{-1} Na_2SeO_4, 1.5 g of n-SiO_2, 0.75 g of Chi, 1 g of Alg, and 7.5 g of UP were dissolved in 34.25 mL of deionized water (to make the total mass of Solution B 50 g) successively according to the procedure described above for Solution B. The prepared Solution B was dripped from a syringe drop by drop into Solution A, which was continuously stirred at a speed of 150 r min^{-1} to produce fertilizer granules. Fertilizer granules were collected after being suspended in Solution A for at least 15 min for sufficient cross-linking. Residual Solution A was removed from the fertilizer granule surface by vacuum filtering for at least 40 min to suppress UP hydrolysis caused by free water in residual Solution A.

2.3. Experimental Design

The content of $CaCl_2$ in Solution A was fixed at 40 mg g^{-1} in this study, while the other components varied according to the experimental design. In particular, neither CMC, n-SiO_2, nor Na_2SeO_4 was used; instead, 15 mg g^{-1} Chi and 20 mg g^{-1} Alg were used in Solution B with variable amounts of UP (100, 150, and 200 mg g^{-1}) in the tentative experiment to explore its influence on the structure.

2.3.1. Single-Factor Experiments of Coating Material

Single-factor experiments were performed to investigate the effect of coating material components on OSR (intensity and sustaining duration). The factor levels of treatments are shown in Table 1:

Table 1. The treatment set of the single-factor experiment.

Factors (Components)	Numbers of Levels	Treatment Levels (Unit: mg g^{-1})
Silicon dioxide nanoparticle (n-SiO_2)	5	0, 10, 20, 30, 40
Alginate (Alg) (in sodium salt form)	3	10, 20, 30
Urea peroxide (UP)	3	100, 150, 200
Chitosan (Chi)	3	10, 15, 20
Carboxymethyl cellulose (CMC)	2	0, 5.0, 10

The contents of the components not being investigated in corresponding assays were set at 10 mg g^{-1} CMC, 15 mg g^{-1} Chi, 10 mg g^{-1} n-SiO_2, 20 mg g^{-1} Alg, and 150 mg g^{-1} UP, while Na_2SeO_4 was still absent in this section. The complete components of these treatments are listed in Table S1.

2.3.2. Multiple-Factor Experiment of Optimal Coating Formulas

An orthogonal design experiment was performed to explore the interaction effect of selected component factors. Three factors significantly affecting OSR, Alg, n-SiO_2, and Chi were selected, and three levels were set for each factor. The factors and corresponding levels were determined based on the results of the single-factor assay. The criteria for this determination are explained in Section 4.1 of the Discussion. Moreover, several formulas named "Control" or "Blank" were also prepared to assess the mechanical and release-control properties of certain components in the formulas. Specifically, the samples of the "Control" group were used in assays concerning both OSR and physical properties (mechanical properties and density), while "Blank" group samples were only subjected to assays of physical properties. The component contents of these treatments are listed in Table 2:

Table 2. The component contents in the multiple-factor experiment.

Treatment Formula Names	Alg	n-SiO_2	Chi	UP	CMC	Na_2SeO_4
	mg g^{-1} (The Mass Proportion of Corresponding Ingredient in Solution)					
I	30	40	20	150	10	0.1
II	25	30	15	150	10	0.1
III	20	20	10	150	10	0.1
IV	25	20	20	150	10	0.1
V	20	30	20	150	10	0.1
VI	30	30	10	150	10	0.1
VII	20	40	15	150	10	0.1
VIII	30	20	15	150	10	0.1
IX	25	40	10	150	10	0.1
Control 1	20	30	15	150	10	0.1
Control 2	20	0	15	150	0	0.1
Control 3	20	30	15	150	10	0.0
Control 4	20	30	15	0	10	0.1
Blank 1	20	30	15	0	10	0.0
Blank 2	20	0	15	150	0	0.0
Blank 3	20	0	15	0	0	0.0

The formula for Control 1 was based on the treatment levels that performed best in peak *Eh*, high *Eh* maintenance duration, or mechanical properties in the single-factor experiment. Blank 1 was to assess the influence of coating material without UP on soil *Eh* and its inherent mechanical characteristics. Control 2 and Blank 2 were prepared to evaluate the effect of n-SiO_2 and CMC on oxidative substances and Se release, as well as granule mechanical properties. Control 3 was used as the blank treatment in investigating the effect of Na_2SeO_4 on granule mechanical properties and inherent Se variation in soil, while Control 4 demonstrated the Se release and transformation in soil without oxidative substances input. Blank 3 provided a reference of pure basic coating materials for mechanical assay.

2.4. Water-Extraction Assay

Ten grams of fertilizer granules were filled into a bag made of 300-mesh nylon. The sealed bag was placed into a polyethylene bottle containing 100 mL of deionized water as a replicate, and three replicates were set for each treatment. The redox potential (*Eh*) of the extraction solution was measured every day by a redox potential meter (Leici YHBJ-262,

INESA Scientific Instrument Co., Ltd., Shanghai, China) equipped with a redox composite electrode (Leici 501, INESA Scientific Instrument Co., Ltd., Shanghai, China) and a temperature electrode (Leici T-818-Q, INESA Scientific Instrument Co., Ltd., Shanghai, China).

2.5. Density Assay of Fertilizer Granules

Two grams (with a precision of 10^{-4} g, m_1) of fertilizer granules were added into a 25-mL (V_0) pycnometer whose mass was m_0. Glycerol was added into the pycnometer to half of its volume, and the pycnometer was gently shaken to make the glycerol sufficiently soak the fertilizer granules and expel the bubbles in the gaps between the granules. Then glycerol was continued to be added until it reached the mouth of the pycnometer, and the lid was covered over the mouth so that excess glycerol overflowed from the capillary in the lid. The total mass (m_2) was weighed after the overflowing glycerol on the pycnometer surface was wiped off with filter paper. The total mass (m_3) of the corresponding pycnometer was weighed after sufficient cleaning and filling only with glycerol again. The density of fertilizer granule, ρ (unit: g cm^{-3}), was calculated by Equation (1) (Its derivation is provided in Appendix A):

$$\rho = \frac{m_1(m_3 - m_0)}{(m_3 - m_2 + m_1)V_0} \quad (1)$$

2.6. Morphological Observation of Fertilizer Granules

A stereoscope (SZ760T, Optec Instrument Co., Ltd., Chongqing, China) equipped with a digital camera (CoolPix P310, Nikon Corporation, Tokyo, Japan) was used for morphological observation and image capture of the corresponding surface and cross-section of fertilizer granules. The intact fertilizer granules were placed in a glass Petri dish, and a piece of black paper was placed between the Petri dish and the sample platform of the stereoscope as a background for observation and image capture. The cross-section of the fertilizer granule was obtained by directly cutting fertilizer granules with a thin blade, and the cross-section was placed face up on the Petri dish. The corresponding observation and image capture were conducted identically to those of the intact granule samples. Some soft samples were frozen with liquid nitrogen before cutting to maintain a satisfactory cross-section. The longest and shortest diameters of fertilizer granules were measured (six sample replicates for each treatment) using ImageJ (version 1.54g) software from the fertilizer granule images after calibration with the ruler image to establish the conversion relationship between pixels and actual length. The intact and cut granule samples subjected to stepwise ethanol dehydration and supercritical fluid CO_2 drying were successively mounted on the copper sample tray using conductive gel for scanning electron microscope (EVO MA 15, Carl Zeiss AG, Oberkochen, Germany) observation after platinum surface coating for conductive treatment.

2.7. Mechanical Assay of Fertilizer Granules

Texture analyzer (TA.XTC-18, Bosin Tech. Co., Ltd., Shanghai, China) equipped with a 35-mm cylinder probe was employed in this assay. An intact fertilizer granule was directly placed in a Petri dish without a cover on the sample trap of the texture analyzer. Each sample was subjected to two pressing cycles with a 15-s interval during analysis: The probe moved downward until 20% deformation of the fertilizer granule occurred, and then it moved upward during every cycle. The probe's moving speeds in both directions were 0.1 mm s^{-1}. Tension data were collected once the pressing force exceeded 25 mN. The parameters of the mechanical assay were defined as below (Figure 1): hardness and the maximum force during first pressing; springiness was defined by Equation (2):

$$\text{springiness} = T_2/T_1; \quad (2)$$

gumminess was defined by Equation (3):

$$\text{gumminess} = A_4/A_1 \times \text{hardness}; \quad (3)$$

and resilience was defined by Equation (4):

$$\text{resilience} = A_3/A_2. \quad (4)$$

Moreover, the relationship among A_1, A_2, A_3 could be expressed as Equation (5)

$$A_1 = A_2 + A_3. \quad (5)$$

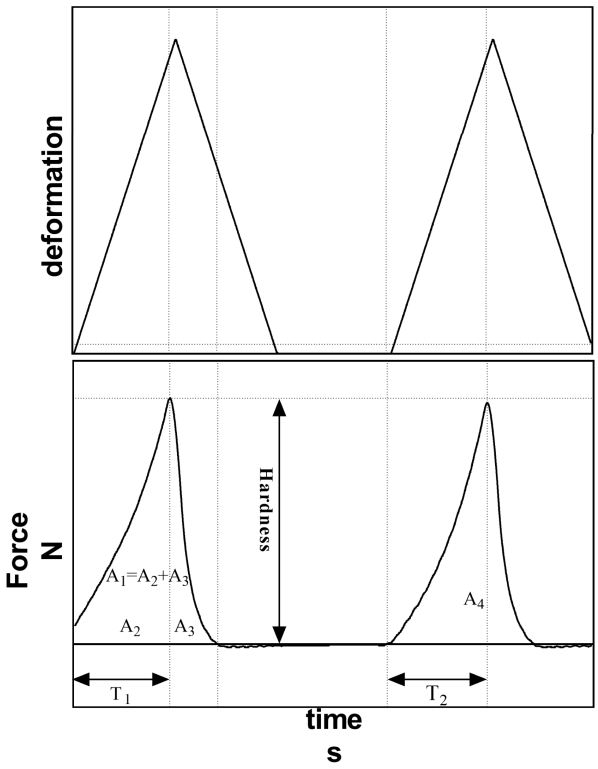


Figure 1. The definition of measured parameters in the tension assay. A_1, the total peak area of the first pressing; A_2, the peak area from data collection beginning to pressing force reaching the maximum value; A_3, the peak area from pressing force reaching the maximum value to the elastic force returning to the baseline; A_4, the total peak area of the second pressing. T_1, the duration from data collection beginning to pressing force reaching the maximum value during the first pressing; T_2, the duration from data collection beginning to pressing force reaching the maximum value during the second pressing.

2.8. X-Ray Diffraction (XRD) Assay

Fertilizer granule samples were dehydrated by ethanol solution successively from 30% to 100% (*v*/*v*). Dehydrated samples in which ethanol had volatilized were ground in a mortar containing liquid nitrogen and a ball grinding mill successively, and the powder was stored in a desiccator with silica gel before assay. XRD scanning, with 2θ ranging from 10° to 70°, was performed by an X-ray diffractometer (Ultima IV, Rigaku Corporation, Tokyo, Japan) with a step length of 0.02° at a speed of 8° min^{-1}.

2.9. Fourier Transform Infrared Spectrophotometry (FTIR)

Fine powder (<2.5 μm) of fertilizer granules was prepared with the identical procedure as the XRD sample. The powder samples were mixed with KBr sufficiently and then

compressed into thin tablets by a hydraulic press. The FTIR scanning was performed with a Fourier transform infrared spectrophotometer (Vertex 70, Bruker Corporation, Rheinstetten, Germany), and the transmittance in the range between 4000 and 400 cm^{-1} was recorded.

2.10. Soil Cultivation Assay

Soil cultivation assay was conducted with selected treatments (Control 1, Control 4, and Treatment II) according to the results of the multiple-factor experiment. In addition, two other treatments, Se (Na_2SeO_4 and urea) and Se + UP (Na_2SeO_4 and UP), were set in this assay as references. The inputs of N and Se nutrients were equal among treatments: 71.4 mg kg^{-1} of N and 65.4 μg kg^{-1} of Se. For details, corresponding fertilizer granules were fertilized with the dose of 1.6 g kg^{-1} in Treatment II and Control 1 treatments; 152 mg kg^{-1} of urea and 1.6 g kg^{-1} of corresponding fertilizer granules were fertilized in Control 4 treatment, 152 mg kg^{-1} of urea and 157 μg kg^{-1} of Na_2SeO_4 were applied in Se treatment, 240 mg kg^{-1} of urea peroxide and 157 μg kg^{-1} of Na_2SeO_4 were applied in Se + UP treatment. This soil cultivation assay was conducted with soil in pots. Each pot contained 7 kg of paddy soil (air-dried basis) in this study, and a 5-cm water layer was maintained on the soil surface during the assay. The fertilizer granules, the reagents Na_2SeO_4, UP, and urea were fertilized evenly into the surface layer (with a depth of around 2 cm) of the submerging paddy soil after sufficient equilibration for water distribution. For Control 4, Se and Se + UP treatments, Na_2SeO_4, UP, and/or urea for N or Se supplementation were directly fertilized into the soil as above. The soil *Eh* was measured regularly by a redox potential meter mentioned in Section 2.4, and the soil was sampled every 20 d since the experiment began.

2.11. Soil Se Speciation Analysis

The soil Se speciation was extracted and determined based on the modified stepwise extraction method of Liu et al. [61]:

Step 1: The air-dried soil sample was ground and passed through a 0.149-mm sieve. Two grammes of ground soil sample were precisely weighed; it was vibrated with 20 mL of 0.25 mol L^{-1} KCl for 1 h at 25 °C at a speed of 200 r min^{-1} in a 50-mL centrifugal tube. The supernatant was collected and filtered through a 0.45-μm filter membrane after 10-min centrifugation at a speed of 4000 r min^{-1} to obtain the water-soluble fraction (Se_{sol}).

Step 2: The precipitate from Step 1 was vibrated with 20 mL of pH 5.0 0.7 mol L^{-1} KH_2PO_4 in a centrifuge tube for 4 h at 25 °C at a speed of 200 r min^{-1}; the supernatant was collected and filtered through a 0.45-μm filter membrane after 10-min centrifugation at the speed of 4000 r min^{-1} to obtain the exchangeable fraction (Se_{exc}).

Step 3: The precipitate from Step 2 was intermittently vibrated with 20 mL of 2.5 mol L^{-1} HCl in a capped centrifuge tube with a 95 °C water bath for 50 min; the supernatant was collected and filtered through a 0.45-μm filter membrane after 10-min centrifugation at a speed of 4000 r min^{-1} to obtain the Fe/Mn oxide-binding fraction ($Se_{Fe/Mn}$).

Step 4: The precipitate from Step 3 was intermittently vibrated with a mixture of 16 mL of 50 g L^{-1} $K_2S_2O_8$ and 4 mL of concentrated HNO_3 in a capped centrifuge tube with a 95 °C water bath for 3 h. The supernatant was collected and filtered through a 0.45-μm filter membrane after 10-min centrifugation at 4000 r min^{-1} to obtain the organic or sulfide binding/ elemental fraction (Se_{ose}).

Step 5: The precipitation from Step 4 was ground to powder whose size was smaller than 0.149 mm (100 mesh) after drying, then it was digested with 10 mL of 4:1 (v/v) HNO_3-$HClO_4$ in polytetrafluoroethylene crucible with 170-°C sand bath until the sample turned white or gray, then 10 mL of 6 mol L^{-1} HCl was added and digestion was continued until the solution volume was evaporated to 2 mL, the digest solution was made up to 25 mL in volumetric flask as residual fraction (Se_{res}).

The Se concentration in the extraction solutions of the above five fractions was determined with an atomic fluorescence spectrometer (AFS-8130, Jitian Instrument Co., Ltd., Beijing, China) using hydride atomic fluorescence spectrometry with 20 g L^{-1} $NaBH_4$ solution as reductant. The tetravalent Se contents (Se^{IV}) of water-soluble, exchangeable, and Fe/Mn oxide-binding fractions and the total Se content (Se_t) were determined directly from the extraction solution, while the Se_t of water-soluble, exchangeable, and Fe/Mn oxide-binding fractions were determined after being reduced by 90~100 °C 6 mmol L^{-1} HCl for 30 min, respectively. The hexavalent Se (Se^{VI}) content was calculated by subtracting the Se^{IV} content from the corresponding Se_t content.

2.12. Statistical Analysis

The results were calculated and expressed in the form of means ± standard errors. The linear regression, analysis of variance, and multiple comparison (by Duncan's new Multiple Range Test) were conducted with R language for Windows (version 4.3.2). A linear model was used in the analysis of variance, and the interaction effects between each pair of two factors (first-order interaction) and among three factors (second-order interaction) were calculated together and expressed as "Alg × Chi × n-SiO_2". The "aov" function, which can handle data whose replicate numbers of treatments and factors were unequal, was applied for analysis of variance since some abnormal observed data were excluded. Moreover, it should be noted that Duncan's Multiple Comparison Test without correction for multiplicity may lead to false-positive results.

3. Results

3.1. The Effect of Fertilizer Components on the Morphological Characteristics of Fertilizer Granules

The tentative assay indicated that the component dissolution sequence during preparation remarkably influenced the fertilizer granule structure. The granules dissolving Alg and Chi first had a finer surface texture and a more spherical shape than those dissolving UP first (Figure S1a,b). Moreover, the one dissolving UP first had larger pores and a larger diameter than the one dissolving Alg and Chi first (Figure S1c,d). Therefore, Alg and Chi were dissolved first in the following preparation.

A remarkable factor affecting fertilizer granule appearance was UP content (Figure 2). The fertilizer granules containing 100 and 150 mg g^{-1} UP had similar diameters (Figure 2a,b). The cross-section of fertilizer with 100 mg g^{-1} UP was substantial but irregularly round (Figure 2d). However, there were considerable numbers of visible large pores in the cross-section of 150 mg g^{-1} UP fertilizer granules, even though their shape was more regularly round (Figure 2e). The addition of 200 mg g^{-1} UP significantly increased fertilizer granule diameter (Figure 2c), and many bubbles appeared in the cross-section, which made the granule surface and cross-section more transparent (Figure 2c,f).

Sample dehydration and drying for scanning electron microscopy amplified the granule structure differences between treatments (Figure S2a,b): The fertilizer granules that dissolved Alg and Chi first had thicker walls with rougher surfaces (Figure S2a), consisting of thick sheets or large blocks (Figure S2c,g), and UP crystals were embedded in the inner wall (Figure S2e,i). In contrast, the granules that dissolved UP first had thinner walls without obvious sheet structure or UP crystals but with smooth blocks (Figure S2d,f,h,j). Notably, the one with 200 mg g^{-1} UP had a more significant honeycomb structure with thinner walls (Figure S3a,b) and a smoother surface with fewer wrinkles (Figure S3c,d,g,h), but no visible embedded UP crystals inside granules (Figure S3e,f,i,j) compared to that with 100 mg g^{-1} UP.

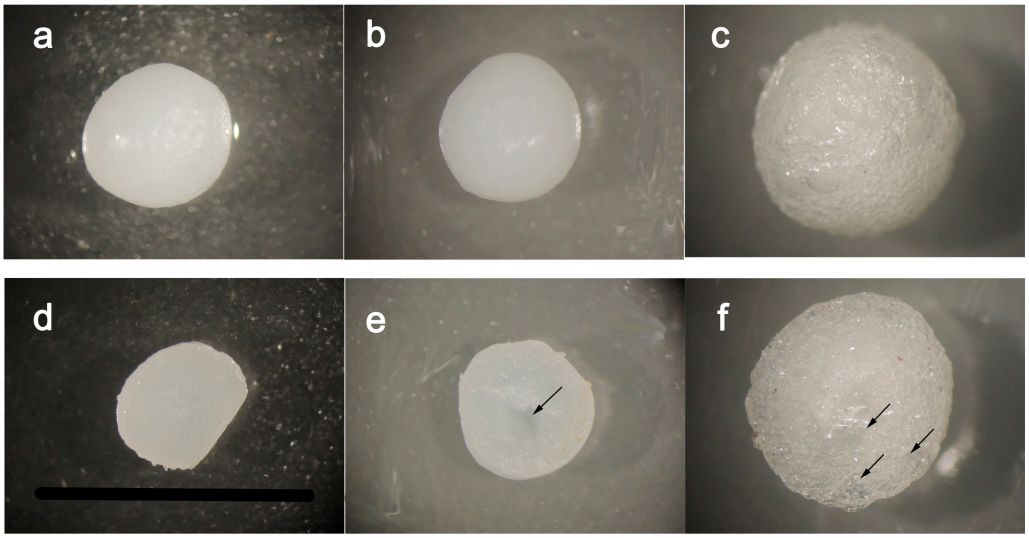


Figure 2. The fertilizer granule with different UP contents. (**a**–**c**), surface appearance; (**d**–**f**), cross-section. (**a**,**d**), 100 mg g^{-1} UP; (**b**,**e**), 150 mg g^{-1} UP; (**c**,**f**), 200 mg g^{-1}. The scale bar was 5 mm. The cavities or encapsulated bubbles in cross-section are indicated by arrows.

To overcome poor shape stability due to fertilizer-structure defects caused by high UP contents (Figures 2 and S2), n-SiO_2 and CMC were added to the formulas to alleviate this problem. The diameter of granules with 10 mg g^{-1} CMC was slightly larger than that without CMC, and their shape was also closer to an orthodox sphere. Moreover, the surface of granules with CMC was smoother, even with some bubbles (Figure 3a,b); moreover, their cross-section was substantial and rougher but without significantly visible cavities or regular texture (Figure 3d). The addition of 10 mg g^{-1} or more n-SiO_2 shifted the granule surface color from lustrously semi-transparent to solid white (Figure S4a–d) and made the cross-section substantial without visible cavities or bubbles (Figure S4e). The longest diameters of fertilizer granules increased with increasing n-SiO_2 content, while the corresponding increase in the shortest diameter was smaller (Figure 4a). The granules with 10 to 30 mg g^{-1} n-SiO_2 could maintain the shape of an orthodox sphere, while the granules with 40 mg g^{-1} n-SiO_2 were oval spheres since the corresponding Solution B was more viscous (Figure S4d,h). For quantitative values, the ratio of shortest diameter to longest diameter of the 40 mg g^{-1} n-SiO_2 treatment was lower than 0.8, while the corresponding values of other treatments were around 0.9. The diameters of fertilizer granules with 10 mg g^{-1} CMC and 10 mg g^{-1} n-SiO_2 increased with increasing UP contents in Solution B (Figures 4c and S5a–c), but UP contents affected the shape of fertilizer granules little (Figure 4d). In any case, the cross-section was still substantial and apparently pore-free even when the UP content reached 200 mg g^{-1} (Figure S5d,e). This result indicated that the addition of CMC and n-SiO_2 could improve the structural stability of fertilizer granules remarkably. The Alg contents also significantly influenced the morphology of fertilizer granules (Figure S6a–c). Since the viscosity of Solution B containing 10 mg g^{-1} Alg was low, the nascent granules formed irregular spheres by gravity during prilling, which resulted in a low shortest diameter (Figure 4e) and shortest diameter–longest diameter values (Figure 4f), and some bubbles were embedded inside granules (Figure S6d). The fertilizer granules were substantial orthodox spheres when the Alg content was 20 or 30 mg g^{-1} (Figure 4f). Moreover, the cross-section of fertilizer granules with 30 mg g^{-1} Alg had a finer and smoother appearance (Figure S6e,f).

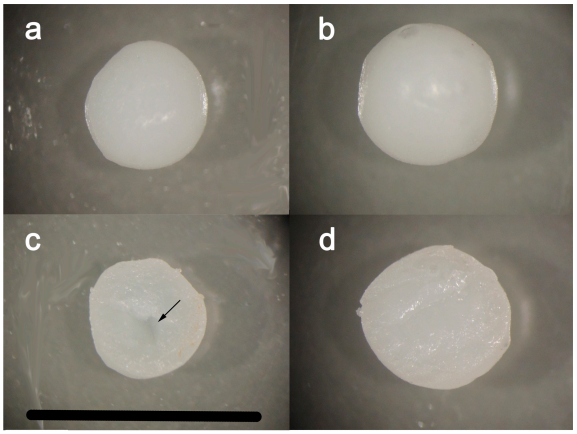


Figure 3. The effect of CMC on coating fertilizer granule structure. (**a**,**b**), surface appearance; (**c**,**d**), cross-section. (**a**,**c**), CMC absent; (**b**,**d**), CMC present. The scale bar is 5 mm. The cavities in cross-section are indicated by arrows.

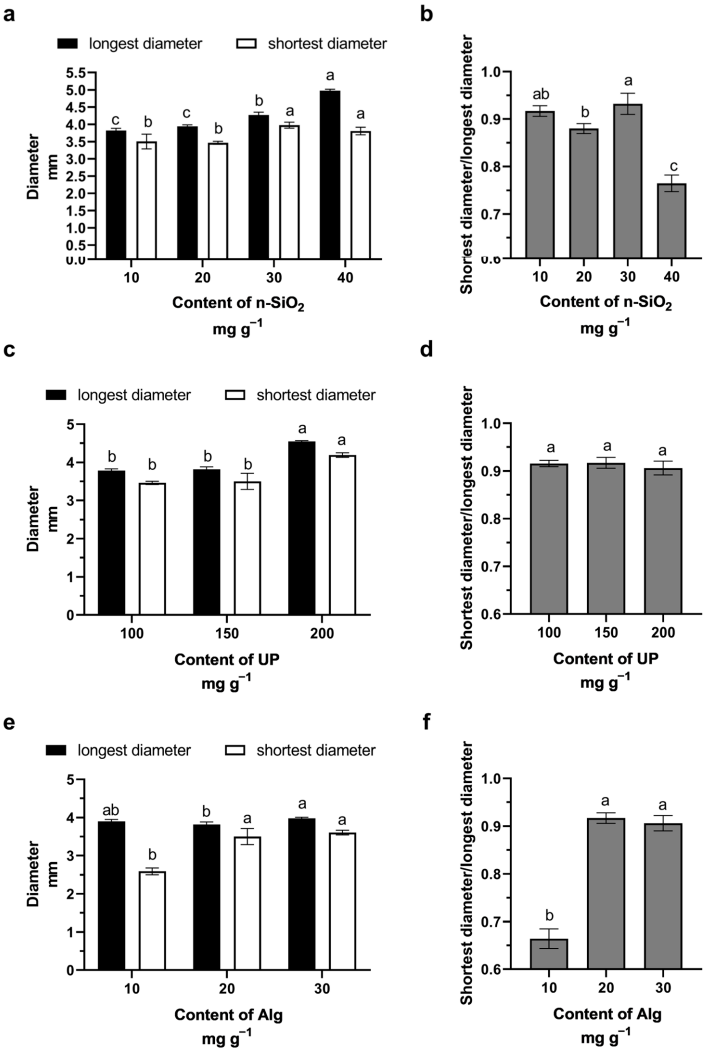


Figure 4. The effect of n-SiO_2, UP, and Alg on coating fertilizer granule size. (**a**,**b**), different n-SiO_2 contents; (**c**,**d**), different UP contents; (**e**,**f**), different Alg contents. (**a**,**c**,**e**), longest and shortest diameters of fertilizer granules; (**b**,**d**,**f**), the ratios of shortest diameter to longest diameter. Data are expressed in the form of mean ± standard error; those followed by the same letters mean the difference between them was statistically insignificant in Duncan's Multiple Comparison Test ($p < 0.05$).

3.2. The Effect of Fertilizer Components on OSR in Water-Extraction Assay

The OSR properties during UP hydrolysis, which were assessed by water extraction, are important indices for evaluating the S/CRF coating effect. The results of the tentative assay indicated that coating led to milder OSR, i.e., slower *Eh* variation and longer high *Eh* (higher than the level of deionized water [LDW]) sustaining duration (HESD) compared to the pure UP treatment without coating, even though the UP contents of the two treatments were identical (Figure S7a). The component dissolution sequence during preparation also determined the OSR properties (Figure S7b): The fertilizer granules dissolving UP first had a sharper and steeper *Eh* curve, in which oxidative substances were completely released within 18 d; whereas the *Eh* curve of those dissolving Alg and Chi first varied mildly and kept at a high value for a longer time. The result of Figure S7c indicated that different UP contents in fertilizer granules showed different *Eh* variation characteristics: the UP content was not closely related to the initial *Eh* values but affected their HESD significantly; the 100 mg g^{-1} treatment lasted 30 d, the 150 mg g^{-1} treatment lasted 37 d, while the 200 mg g^{-1} treatment lasted 57 d. Moreover, the highest *Eh*, as well as the corresponding ascending and descending rates of the 150 mg g^{-1} and 200 mg g^{-1} UP treatments, were significantly higher than those of the 100 mg g^{-1} treatment. Interestingly, the proportion of the slow descending stage after reaching the peak within the total HESD increased from 35.5% for the 100 mg g^{-1} treatment to 61.0% for the 200 mg g^{-1} treatment. In any case, the OSR characteristics of the formulas with n-SiO_2 and CMC were different from those without n-SiO_2 and CMC (Figure 5).

Higher UP content led to longer HESD as expect: Extraction solution *Eh* of three treatments reached 600 mV within 1 d since the experiment began, and kept 30 d (100 mg g^{-1}- or 150 mg g^{-1}-UP treatment) to 45 d (200 mg g^{-1}-UP) before they suddenly decreased to LDW when there were 10 mg g^{-1} n-SiO_2, 10 mg g^{-1} CMC, 15 mg g^{-1} Chi, and 20 mg g^{-1} Alg in the formulas (Figure 5a).

The fertilizer granules with 10 mg g^{-1} Alg depleted their oxidative substances after 19 d, which was shorter than the other two treatments with higher Alg contents. In the comparison between 20 mg g^{-1}- and 30 mg g^{-1}-Alg treatments, the *Eh* values of 30 mg g^{-1}-Alg treatment were always lower than 20 mg g^{-1}-Alg treatment during the first 25 d, but the former one still maintained a high *Eh* level while the latter one had begun to decrease during from the 25th to 30th day under the condition that the formulas contained 150 mg g^{-1} UP, 10 mg g^{-1} CMC, 15 mg g^{-1} Chi, and 10 mg g^{-1} n-SiO_2 (Figure 5b). In other words, the 20 mg g^{-1}-Alg treatment had a higher peak *Eh* but shorter HESD, while the 30 mg g^{-1}-Alg treatment had longer HESD with milder OSR.

The n-SiO_2 content affected the highest *Eh* value little but affected HESD remarkably when there were 150 mg g^{-1} UP, 10 mg g^{-1} CMC, 15 mg g^{-1} Chi, and 20 mg g^{-1} Alg in the formulas. The initial *Eh* values of all treatments with n-SiO_2 were elevated differently, while the corresponding HESD was shortened compared to that without n-SiO_2. The longest HESD occurred at the 30 mg g^{-1} n-SiO_2 treatment among the four treatments with n-SiO_2 (Figure 5c).

The high *Eh* status of 10 mg g^{-1}, 15 mg g^{-1}, and 20 mg g^{-1} Chi treatments could be maintained for 27, 16, and 29 d when the formulas contained 150 mg g^{-1} UP, 10 mg g^{-1} CMC, 2 mg g^{-1} Alg, and 10 mg g^{-1} n-SiO_2, respectively. A sharp *Eh* drop to below 390 mV occurred between the 27th and 30th day for the 10 mg g^{-1} and 20 mg g^{-1} Chi treatments, whose patterns were similar. On the other hand, the decline of the 10 mg g^{-1} Chi treatment was milder during the 16th to 32nd day. In any case, the HESD of the 10 mg g^{-1} Chi treatment was also shorter than that of the 15 mg g^{-1} treatment, even though the phenomenon in which *Eh* decreased after a slight increase occurred in both treatments, and the plateau

stage after *Eh* reached LDW appeared only in the 10 mg g^{-1}- and 15 mg g^{-1} Chi treatments (Figure 5d).

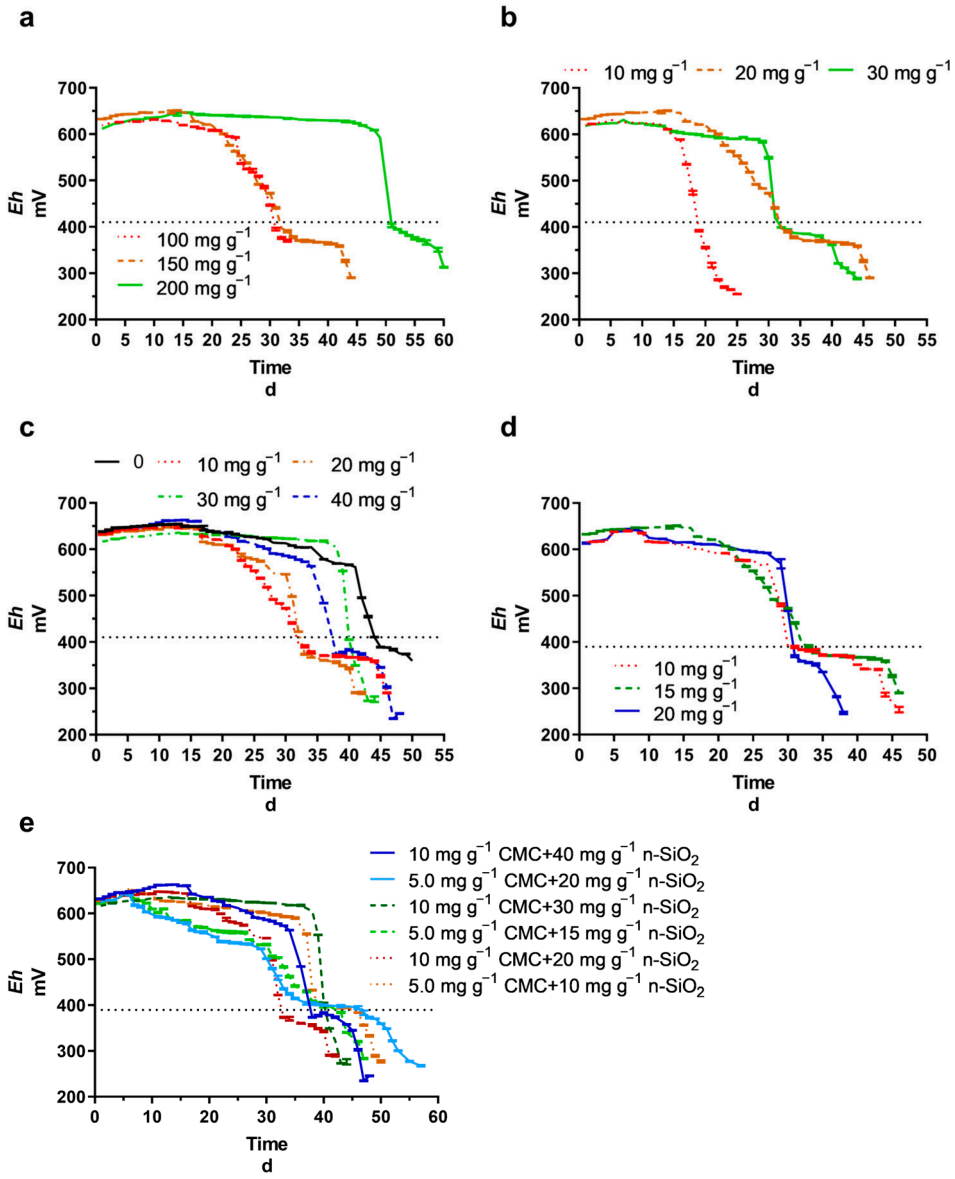


Figure 5. The effect of components in fertilizer granules on water-extraction redox potential (*Eh*) variation in a single-factor assay. (**a**), different UP contents; (**b**), different Alg contents; (**c**), different n-SiO_2 content; (**d**), different Chi content; (**e**), different CMC/SiO_2 ratio. The dotted lines indicate the *Eh* level of deionized water.

Since both CMC and n-SiO_2 acted as permeation regulators in fertilizer, the effect of their ratio (CMC/SiO_2) for OSR was also investigated under the condition that the formulas contained 150 mg g^{-1} UP, 10 mg g^{-1} CMC, 15 mg g^{-1} Chi, and 20 mg g^{-1} Alg (Figure 5e). Similar to the result of Figure 5c, the longest HESD occurred in the 1:3-CMC/n-SiO_2 treatments (10 mg g^{-1} CMC + 30 mg g^{-1} SiO_2 and 5.0 mg g^{-1} CMC + 15 mg g^{-1} SiO_2). However, higher peak *Eh* occurred in the treatments with 1:2-(i.e., 5.0 mg g^{-1} CMC + 10 mg g^{-1} SiO_2) rather than 1:4-CMC/n-SiO_2 (i.e., 5.0 mg g^{-1} CMC + 20 mg g^{-1} SiO_2) among the treatments with 5.0 mg g^{-1} CMC, which was different from the results of the products containing 10 mg g^{-1} (CMC 10 mg g^{-1} CMC + 20 mg g^{-1} SiO_2 and 10 mg g^{-1} CMC + 40 mg g^{-1} SiO_2). Except for the case of 1:2-CMC/SiO_2 (10 mg g^{-1} CMC + 20 mg g^{-1} SiO_2 and 5.0 mg g^{-1} CMC + 10 mg g^{-1} SiO_2), higher absolute contents of CMC and n-SiO_2

led to longer HESD and higher peak *Eh* among the treatments with the same CMC/SiO_2. In summary, the OSR performance of fertilizers with 10 mg g^{-1} CMC was better than those with 5.0 mg g^{-1} CMC. In addition, remarkably low fluidity was observed in Solution A with 15 mg g^{-1} CMC in a preliminary experiment in our assay, which made removing residual free water from the granule surface more difficult. Therefore, it could be assumed that 10 mg g^{-1} was the proper CMC content for further study.

3.3. The Effect of Components on the Mechanical Properties of Fertilizer Granules

After determining the preliminary formula of fertilizer granules according to OSR, it is necessary to analyze the contribution of components in this formula to mechanical properties. Some treatments (four "Control" treatments and three "Blank" treatments) listed in Table 2 were used to analyze the effects of these factors. Quantitative results of mechanical assays suggested that n-SiO_2 and CMC significantly enhanced the hardness and gumminess of fertilizer granules compared to those in which n-SiO_2 and CMC were absent (Control 2, Blank 2 and 3) (Table 3). Moreover, UP addition slightly decreased the hardness and gumminess of granules containing Alg, Chi, n-SiO_2, and CMC but without Na_2SeO_4 (Control 3 versus Blank 1, Control 1 versus Control 4), while its effect was not obvious when n-SiO_2 and CMC were absent (Blank 2 versus Blank 3). On the other hand, UP lowered the springiness remarkably when Na_2SeO_4 was absent (Control 3 versus Blank 1, Blank 2 versus Blank 3), but n-SiO_2 and CMC increased it mildly (Control 1 versus Control 2, Control 3 versus Blank 2, Blank 1 versus Blank 3). Interestingly, Na_2SeO_4 led to higher hardness, gumminess, and resilience, but lower springiness, which was more remarkable when n-SiO_2 and CMC were in the formulas (Control 1 versus Control 3, Control 4 versus Blank 1). In any case, the lowest gumminess occurred in the Control 2 formula even with Na_2SeO_4. UP played a positive role for resilience when n-SiO_2 and CMC were absent (Blank 2 versus Blank 3), so the formula with only Alg, Chi, and UP, i.e., Blank 2, had the highest resilience; but UP had little effect when n-SiO_2 and CMC were present. The effect of n-SiO_2 and CMC on resilience was not generally distinguishing. In addition, Na_2SeO_4 reduced granule resilience to around 80% of the level of the treatment with Alg, Chi, and UP in this study (Blank 2 versus Control 2). Considering the crucial mechanical properties (hardness and resilience) in this study, it could be assumed that the formula based on the results of the single-factor assay (20 mg g^{-1} Alg, 15 mg g^{-1} Chi, 10 mg g^{-1} CMC, 30 mg g^{-1} SiO_2, 150 mg g^{-1} UP, and 0.1 mg g^{-1} Na_2SeO_4), i.e., Control 1, performed fairly ideally in this assay.

Table 3. The mechanical properties of blank and control treatments.

Names of Treatment Formula	Hardness N	Springiness	Gumminess N	Resilience
Control 1	1.104 ± 0.032 a	0.718 ± 0.021 bc	0.780 ± 0.026 a	0.251 ± 0.004 b
Control 2	0.274 ± 0.013 c	0.685 ± 0.020 c	0.160 ± 0.011 d	0.243 ± 0.012 b
Control 3	0.810 ± 0.048 b	0.768 ± 0.025 bc	0.486 ± 0.018 b	0.216 ± 0.004 c
Control 4	0.960 ± 0.049 ab	0.899 ± 0.010 a	0.710 ± 0.026 a	0.237 ± 0.005 b
Blank 1	0.824 ± 0.033 b	0.867 ± 0.011 a	0.546 ± 0.018 b	0.211 ± 0.004 c
Blank 2	0.314 ± 0.014 c	0.672 ± 0.022 c	0.216 ± 0.011 c	0.286 ± 0.010 a
Blank 3	0.300 ± 0.012 c	0.789 ± 0.017 b	0.218 ± 0.012 c	0.204 ± 0.004 c

Data are expressed in the form of mean ± standard error; those followed by the same letters mean the difference between them was statistically insignificant in Duncan's Multiple Comparison Test ($p < 0.05$).

Apart from analyzing how the component affected mechanical properties, it was meaningful to conversely optimize the formula of fertilizer granules with orthogonal design

treatments (Control 1 and Treatments I to IX in Table 2) after investigating their mechanical properties. In the multiple-factor assay (Figure 6), the highest hardness and gumminess were observed in the Control 1 formula, while Treatments I, V, and VIII also had high hardness. Moreover, Treatments III, VI, and IX, with low hardness and gumminess, were highly resilient; furthermore, Treatments III and IX were also the least springy among treatments in the orthogonal design experiment. Moreover, Treatment IV, with medium hardness and gumminess, had high springiness but low resilience. The analysis of variance indicated that there were interaction effects among the contents of Alg, Chi, and n-SiO_2 for hardness, gumminess, and resilience. Therefore, it was more appropriate to infer the optimal formula from the multiple comparison results for specific treatments than from the comprehensive results for the levels of each factor, in view of statistical theory.

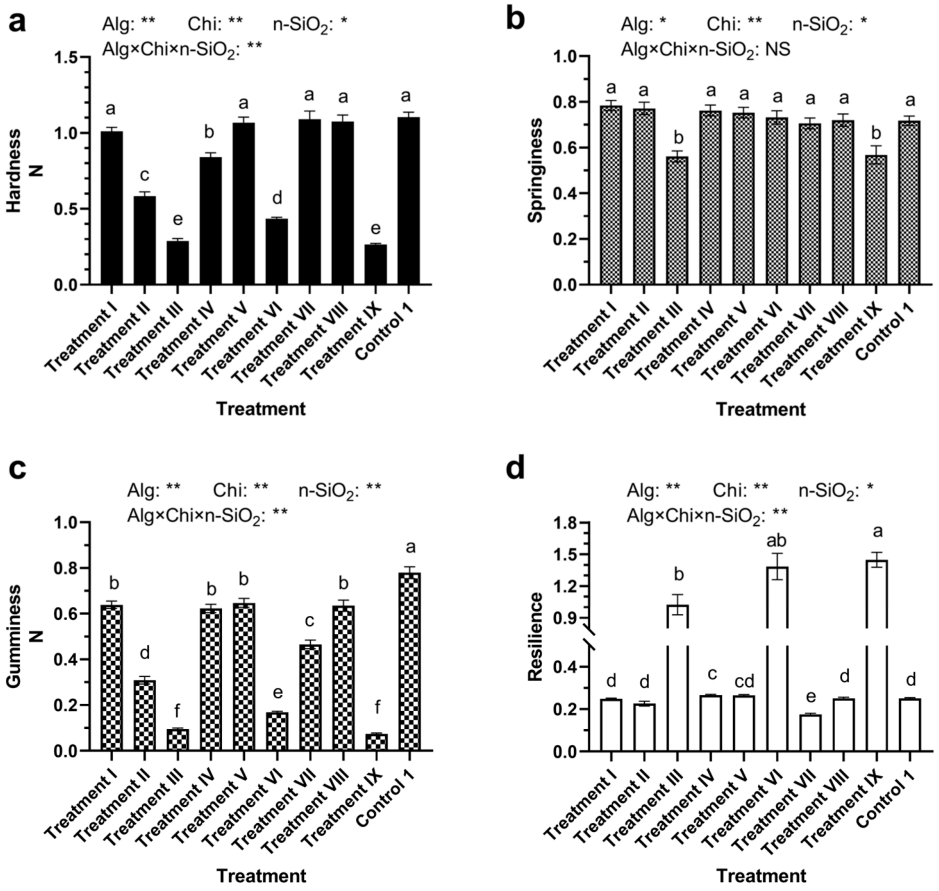


Figure 6. The mechanical properties of fertilizer granules in an orthogonal design experiment. (**a**), hardness; (**b**), springiness; (**c**), gumminess; (**d**), resilience. Data are expressed in the form of mean ± standard error; those followed by the same letters mean the difference between them was statistically insignificant in Duncan's Multiple Comparison Test ($p < 0.05$). Asterisks indicate significance of factor effects or interaction effects among factors verified by analysis of variance; * means $0.01 \leq p < 0.05$, ** means $p < 0.01$, while NS means insignificant ($p > 0.05$). The details of the analysis of variance are shown in Table S2.

Although significant ($p < 0.05$) linear correlation only occurred between gumminess and hardness among blank and control treatments, significant linear correlations existed between each pair of parameters among nine orthogonal design treatments and the Control 1 (Figure S8), which meant that the correlation between gumminess and hardness was inherent, i.e., additive (n-SiO_2, CMC, UP, etc.)-independent, in the Alg–Chi compound coating material; while other correlations between investigated parameters, especially those related to resilience, were established only when all components existed in the formula

simultaneously. Moreover, the results of Figures 6 and S8 also implied that fertilizer granules with high hardness could maintain their shape within wide elastic deformation ranges, but they were difficult to recover to their original shapes after being subjected to forces exceeding their springiness limit.

3.4. Fertilizer Granule Density

The result of Figure 7 indicates that the density of the fundamental coating material (Blank 3) was slightly higher than 1.00 g cm^{-3}, and the UP addition (Blank 2) significantly decreased fertilizer granule density to 0.70 g cm^{-3}, which coincided with the morphological results of Figures 2 and S3. In any case, the addition of n-SiO_2 and CMC (Control 1) remarkably reversed this trend and restored the product density to 1.06 g cm^{-3}, but it was still lower than the complete coating material formula (Blank 1). Interestingly, not only the mechanical properties mentioned above but also the granule density were remarkably improved by Na_2SeO_4, although it was added only at the 1/10,000-scale (Control 2).

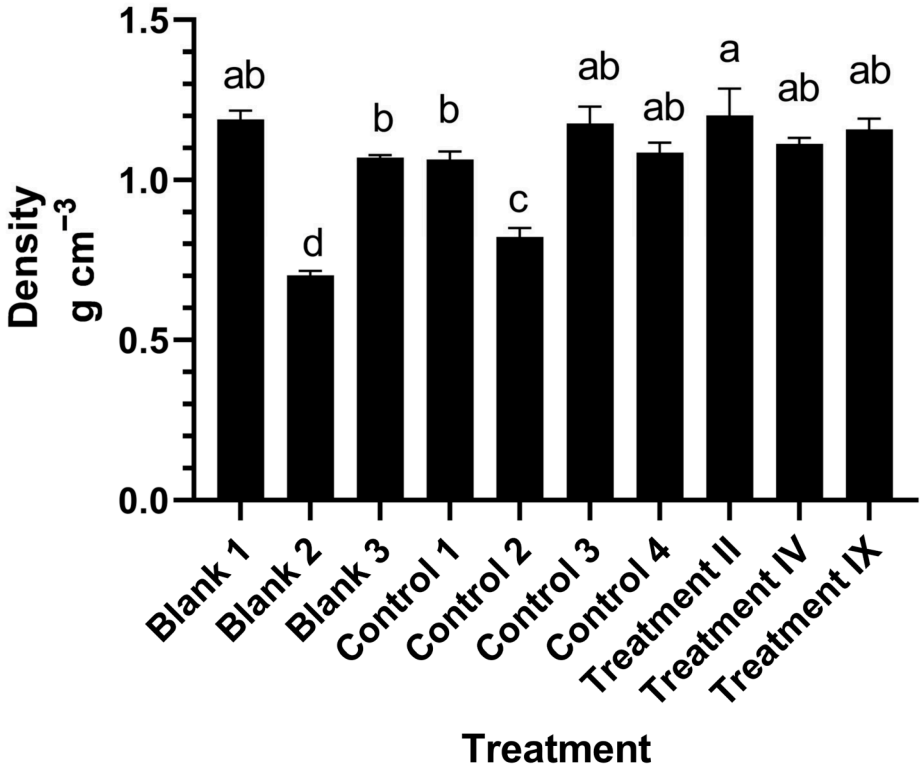


Figure 7. The density of fertilizer granules of representative treatments. Data are expressed in the form of mean ± standard error; those followed by the same letters mean the difference between them was statistically insignificant in Duncan's Multiple Comparison Test ($p < 0.05$).

3.5. The Treatment OSR of Orthogonal Design in Water Extraction and Soil Cultivation Assays

In single-factor assays (Figures 5 and S7), the *Eh* curves of treatments overlapped each other, which made it difficult to discriminate satisfactory treatments. It is predictable that this problem became more severe in orthogonal design experiments since their formulas were more similar. Therefore, fertilizer granules that had been stored for 6 months after preparation were used in this section to amplify the OSR difference among treatments. The *Eh* values of all treatments were lower than LDW (340.7 mV) during almost the entire assay (Figure 8a). Moreover, an obvious *Eh* drop to below −100 mV occurred on the 2nd or 3rd day for almost all treatments, which did not happen in previous assays with newly prepared fertilizers (Figure 5); however, the *Eh* drop of Treatment V was less significant

as an exception. Moreover, the early-stage *Eh* curve valleys of Control 1 and Treatment IX happened later, at the 6th and 12th day, respectively. Figure 8a also suggested that several treatments (Treatment I to IV, VIII, IX, and Control 1) recovered to 100~200 mV after the 10th day, while the corresponding values of Treatment V to VII remained fluctuating at levels lower than 100 mV. For details, the *Eh* curves of the Control 1 and Treatment II treatments almost overlapped each other, and their HESD was over 60 d. Moreover, the low-*Eh* status of Treatment IV remained until the 20th day, then fluctuated between 100 and 250 mV. In any case, the *Eh* values of Treatment V and VII were over 150 mV during the first 15 d, but they declined and continued to vary below 100 mV, with the lowest *Eh* values reaching −44.4 mV and −160.7 mV, respectively. This phenomenon indicated that the component variation not only influenced the peak value and HESD but also determined the length of the low-*Eh* period before ORS from inside the fertilizer granules began (delay period).

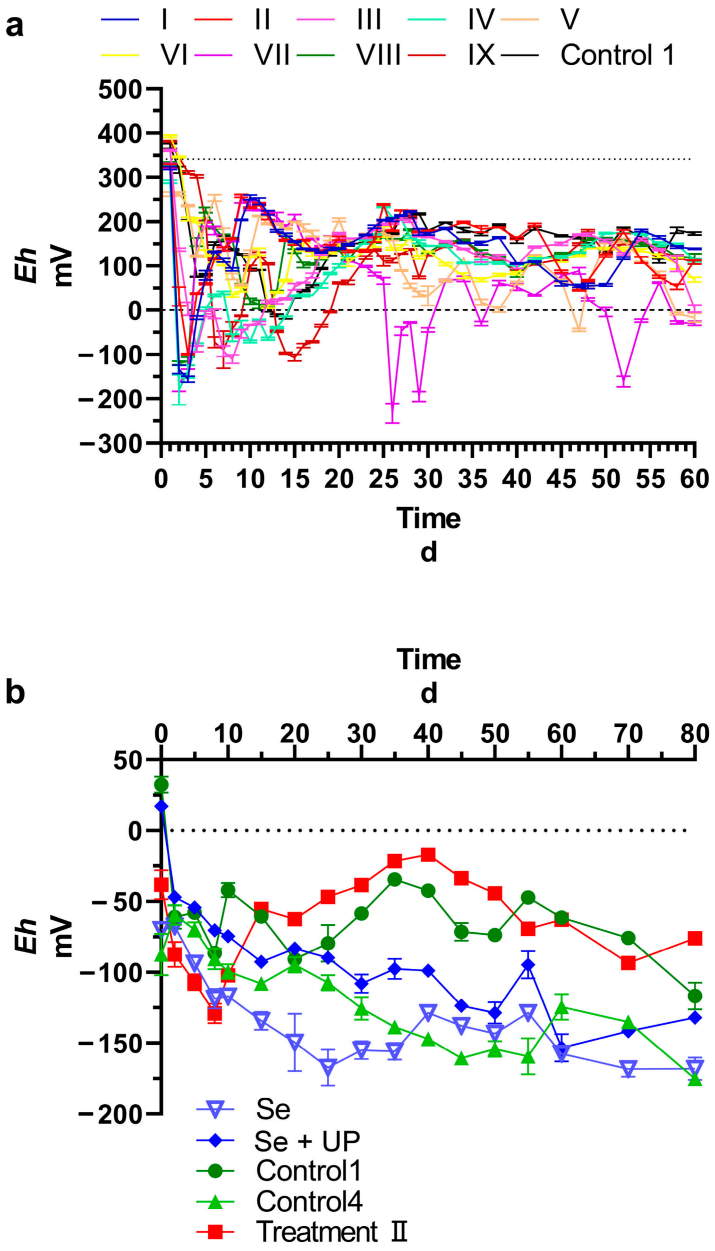


Figure 8. The *Eh* values of treatments based on orthogonal design in (**a**) water-extraction assay and (**b**) selected treatments in soil cultivation assay. The dashed line in figures indicated the *Eh* level of 0 mV.

The soil cultivation assay results (Figure 8b) coincided with those in the water-extraction assay (Figure 8a), although the absolute values were lower. The treatments that were able to maintain high *Eh* for a long duration in the water-extraction assay (Control 1, Treatment II) also elevated soil *Eh* to a higher level than the treatments whose *Eh* values were low in the water-extraction assay. A common *Eh* drop occurred during the first 8 d of the assay, with the lowest values among these treatments ranging from −86.5 mV to −129 mV. Then, the *Eh* values of treatments varied diversely: The Se treatment *Eh* continued declining until the 25th day and fluctuated between −128.8 mV and −168.8 mV later. The *Eh* values of the Se + UP treatment also decreased in the short term and then increased slightly; in any case, its rate of decline was slower than the Se treatment, and its lowest value was around 150 mV, which was always higher than the corresponding values of the Se treatment during the entire assay. The treatment in which only Na_2SeO_4 was embedded in the coating material, and UP was absent, i.e., Control 4, showed an *Eh* pattern similar to that of the Se + UP treatment during the first 30 d and from the 60th to the 80th day, but its *Eh* variation during the 35th to 50th day was closer to the Se treatment. The *Eh* variation patterns of Control 1 and Treatment II were generally similar but with subtle differences: The *Eh* values of both treatments were higher than the other three treatments since the *Eh* drop during the first 8 d had passed, and their *Eh* values recovered to their peaks during the assay between the 35th and 40th day. The initial *Eh* value of Control 1 was 32.3 mV, while that of Treatment II was −38.2 mV; however, the Control 1 *Eh* was higher than that of Treatment II only during the first 10 d and from the 55th to the 70th day; the latter rise did not occur for Treatment II; in contrast, the *Eh* fluctuation of Control 1 was gentler than that of Treatment II.

3.6. XRD Analysis

Typical X-ray diffraction patterns of raw UP and Na_2SeO_4 were observed. However, the polymerization degrees of CaAlg and Chi were diverse, and they lacked crystallization conditions during cross-linking and solidification; moreover, the crystal structure and anisotropy of n-SiO_2 seemed to be significantly weakened by nanoparticle preparation, although it was a pure compound. Consequently, the diffraction pattern of CaAlg, Chi, and n-SiO_2 lacked sharp peaks (Figure S9a). Moreover, the fine-crystal UP and Na_2SeO_4 were distributed evenly and randomly in the matrix gel, which led to diffraction ray scattering. Therefore, the matrix of fertilizer granules and final products also exhibited an amorphous diffraction pattern; i.e., the distinguishing characteristic peaks were masked by some broad peaks in these patterns (Figure S9b,c). Thus, these amorphous diffraction patterns would mask the potential subtle pattern variations (new peaks and intrinsic peak shifts), making it difficult to recognize whether new substances were produced during fertilizer preparation. Therefore, FTIR was applied to reveal the structural basis of the differences among treatments in OSR and mechanical properties from another perspective.

3.7. FTIR Analysis

It was surprising that one of the most distinguishing peaks of the FTIR pattern originated from n-SiO_2 (474 and 1108 cm^{-1} for pure SiO_2 [Figure 9a] and shifted to 472 ± 2 and 1106 ± 1 cm^{-1} in final products [Figure 9b], respectively). This meant that although it could not be detected by XRD, n-SiO_2 did contribute to maintaining fertilizer granule structure by its Si-O bond. Moreover, the absorbance peak at 1427 cm^{-1} from carboxyl groups of CaAlg and CMC was also found in all treatments, including the blank and control ones (shifting to 1422 cm^{-1} at maximum) as proof of their skeleton function (Figure 9a–c). Notably, a remarkable shift occurred in the n-SiO_2 peak originally at 803 cm^{-1} (Figure 9a), which often appeared in the range between 809 and 814 cm^{-1} in most treatments (Figure 9b,c).

This phenomenon indicated that the asymmetric stretching vibration of SiO_2 was further reduced after the composition of the coating material. Moreover, there were asymmetric stretching vibration peaks of amorphous n-SiO_2 and the peak of carboxylic acid groups from CMC and Alg in the range of 1050~1110 cm^{-1}; absorption peaks (Figure 9a) in this range were observed in almost all treatments except Blank 2, owing to an overlapping effect (Figure 9b,c). Similarly, the bond between -COO^- and -NH_4^+ with an absorption peak at 1602 cm^{-1} from Chi, CMC, and Alg also shifted to the range between 1606 and 1612 cm^{-1} (Figure 9a–c). The patterns of treatments in the orthogonal design assay were similar, but there were some subtle differences in the ranges between 3150 and 3350 cm^{-1} (Figure 9c), which included the absorption peaks caused by the interaction between the -OH and -NH_2 groups of Alg, Chi, and CMC and the -O-O- groups in UP (Figure 9a). In addition, this phenomenon was more remarkable among blank and control treatments (Figure 9b). Notably, the characteristic absorption peak of SeO_4^{2-} at 887 cm^{-1} (Figure 9a) was not prominent in the product patterns (Figure 9b,c).

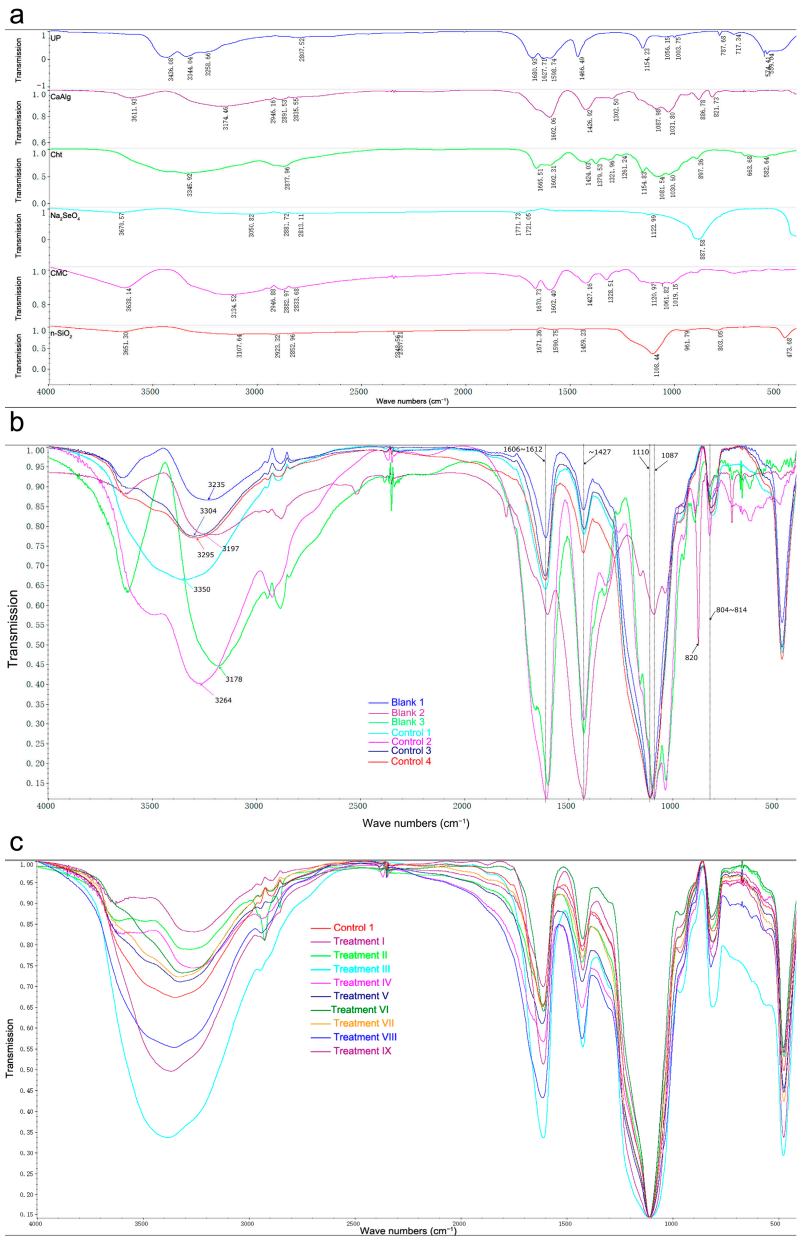


Figure 9. Fourier transform infrared spectra (FTIR) of (**a**) raw material, (**b**) blank and control treatments, as well as (**c**) treatments based on orthogonal design.

3.8. Soil Se Fractions Variation of Selected Treatments

Since the selenate content was on the order of 10^{-4}, it is meaningful to explore whether the Se in the fertilizer granules alters the soil Se condition.

The contents of almost all Se fractions, except Se_{ose}, of all treatments, increased to varying degrees during the first 20 d of this assay due to exogenous Se input (Figure 10a–e). On the contrary, the Se_{ose} contents and proportions of almost all treatments were lower than their corresponding initial values during the whole assay (Figure 10e,f). Specifically, soluble Se_t and Se^{VI} contents of Se treatment increased most significantly among treatments (Figure 10b); Se_{exc} of all treatments increased remarkably (Figure 10f), and Se_t and Se^{VI} of Se_{exc} as well as Se_{res} of Se + UP treatment were highest among treatments at that time (Figure 10c,e). In addition, Treatment II had the highest Se_t and Se^{VI} of the Fe/Mn-binding fraction and total soil Se (Figure 10a,d), which also made it the treatment with the highest total soil Se (Figure 10a); while the Control 1 treatment resulted in the highest Se_{ose} content (Figure 10e).

On the 40th day, the highest content of soluble Se_t belonged to the Se + UP treatment. The treatment whose soluble Se^{VI} remained at a high level was Control 1, while the Se_{sol} of other treatments generally decreased; i.e., the dominant valence of Se_{sol} in the Se + UP treatment was also tetravalent (Figure 10b). The exchangeable Se_t and Se^{VI} faction contents and proportions of the three coated fertilizer treatments kept increasing, and Control 1 was the treatment with the highest values of these two parameters at that time; meanwhile, the corresponding parameters of Se and Se + UP treatments decreased (Figure 10c,f). Although the $Se_{Fe/Mn}$ contents of Se and Se + UP were higher than those of the three coated fertilizer treatments, the major Se form of the former two treatments was Se^{IV} with low phytoavailability (Figure 10d). In addition, the Se_{ose} of the Se treatment and Treatment II increased remarkably at the 40th day (Figure 10e). Moreover, the Se_{res} contents and proportions of all treatments increased to different scales, with the maximum values of residual and total soil Se occurring in the Se + UP treatment (Figure 10a,e,f).

A general increment was observed in Se_{sol} (both absolute values and proportions) of all treatments at the 60th day; Treatment II had the highest Se_t and Se^{VI} of the soluble fraction (Figure 10b,f); moreover, its exchangeable Se_t and Se^{VI} stayed at relatively high levels when the corresponding values of other treatments had declined (Figure 10c). Notably, Control 4 treatment successfully maintained its Se_t and Se^{VI} of $Se_{Fe/Mn}$ as well as Se_{res} at high levels, while the corresponding parameters of other treatments generally declined (Figure 10d,e). Similarly, Control 1 treatment, whose Se_{ose} was highest among treatments, showed the smallest decline (Figure 10e).

The total soil Se contents converged at the 80th day (Figure 10a). However, the Se_{sol} contents of treatments varied diversely, while Se_{ose} generally decreased. In any case, the Se_t and Se^{VI} of the soluble fraction, exchangeable Se_t, as well as the Se_{ose} fraction of Treatment II were the highest among treatments (Figure 10b,c,e). Meanwhile, the Se^{VI} contents of Se_{exc} and $Se_{Fe/Mn}$ of Control 1 were the highest, with significant increases in the corresponding parameters among treatments. The Fe/Mn-binding Se_t contents of all treatments increased to varying degrees, with the highest for the Se + UP treatment (Figure 10c,d). For Se_{res}, the three coated fertilizer treatments decreased while Se and Se + UP treatments increased; the highest Se_{res} occurred in Se treatment (Figure 10e).

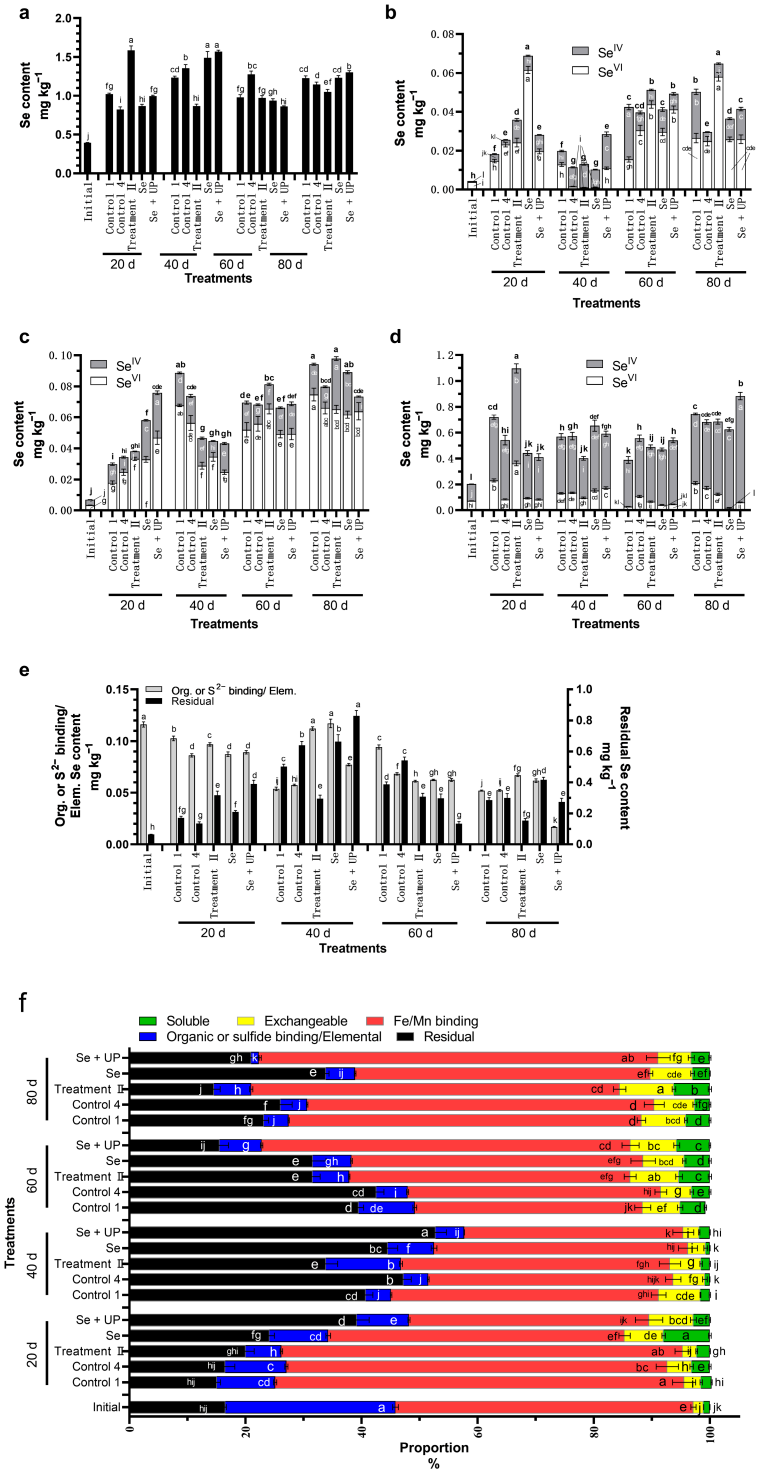


Figure 10. Soil Se fraction concentrations of selected treatments in soil cultivation assay. (**a**), total Se concentration; (**b**), soluble Se fraction; (**c**), exchangeable Se fraction; (**d**), Fe/Mn-binding fraction; (**e**), organic sulfide/elemental and residual Se fraction; (**f**), Se fraction proportion. The tetravalent Se (Se^{IV}) and hexavalent Se (Se^{VI}) contents of soluble, exchangeable, and Fe/Mn-binding fractions were also shown in corresponding panels. Data are expressed in the form of mean ± standard error; data followed by the same letters mean the difference between corresponding parameters was statistically insignificant in Duncan's Multiple Comparison Test ($p < 0.05$). The plain letters inside columns indicate the significance of the corresponding fractions (e.g., Se^{IV} of Se_{sol}, Se^{VI} of Se_{exc}, or the proportion of $Se_{Fe/Mn}$ in Initial treatment), while the bold letters at the top of columns indicate the significance of the total concentrations of corresponding parameters.

4. Discussion

4.1. The Selection of Factors and Levels for Orthogonal Design Experiment

Although all components affected the mechanical and OSR properties and were worthwhile investigating further, the number of factors and levels in the orthogonal design experiment is limited, so the factors and corresponding levels for further study need to be selected based on the single-factor assay. Both mechanical properties and OSR pattern were important criteria for factor selection. According to previous assays (Figures 5 and S7), higher UP content led to longer HESD as expected, which was easy to predict. In addition, the potential structural defect caused by high UP content could be overcome by the addition of n-SiO_2 and CMC (Figures 3 and S5), and the presence of UP did not remarkably influence the hardness of fertilizer granules, which was the essential mechanical parameter we were concerned with, when n-SiO_2 and CMC were present (Table 3), so UP content was no longer a critical factor restricting formula adjustment. Moreover, according to the results of Section 3.2, the effect of CMC on OSR was relatively clear, and the optimal concentration, 10 mg g^{-1}, could be determined based on the single-factor assay (Figure 5c).

By contrast, there was more exploring space for the effects of Alg, Chi, and n-SiO_2 contents: since the Solution B with 10 mg g^{-1} Alg led to fertilizer granules with poor shape (Figures 4e and S6), and both 20 mg g^{-1}- and 30 mg g^{-1}-Alg treatments had their respective advantages in OSR in the single-factor assay (Figure 5b), the Alg contents in the multiple-factor assay (i.e., orthogonal design experiment) for the optimal formula were set as 20, 25, and 30 mg g^{-1}. Similarly, the *Eh* curves of three levels of Chi contents in the single-factor assay (Figure 5c) were quite close to each other: lower Chi content led to longer HESD, while higher Chi content could achieve a higher peak *Eh* at the initial stage, which was worth further investigation. Therefore, these three levels of Chi content—10, 15, and 20 mg g^{-1}—were selected for the orthogonal design experiment. Although Figures 4b and 5d indicated that 30 mg g^{-1} n-SiO_2 led to satisfactory morphological performance (the highest shortest diameter/longest diameter, which meant that the fertilizer granules were "more orthodox" spheres) and OSR, the nonlinear rather than linear effect of n-SiO_2 content on OSR suggested that there might be more complicated interaction effects when the contents of Alg, Chi, and n-SiO_2 were altered simultaneously. Therefore, 20, 30, and 40 mg g^{-1} were chosen as the levels of the n-SiO_2 content factor in the orthogonal design experiment. We had to acknowledge that these selected factors and corresponding levels in this study might not be the best choice, but at least a proper one.

4.2. Release Properties Influenced by Coating Material Formula

The cross-linking process determines release properties since it affects the stability, i.e., decomposition resistance, of coating material polymers [62], thereby allowing coated substances to be released according to the designed pattern under given conditions (e.g., specific pH or soil moisture) [5,62]. The properties of CaAlg obviously depend on the concentration ratio of Ca^{2+} and Alg: Interpolyelectrolyte complexes exhibited better corrosion resistance than the corresponding single substances. The conformational alteration of macromolecules with high polymerization degree after cross-linking contributes to the high anti-deformation ability and pseudoplastic fluid characteristic of Chi–Alg and Chi–CMC complexes [63], which was verified by the results of mechanical assay (Table 3). The electrostatic interaction between Ca^{2+}, -NH_3^+ (from Chi), and -COO^- (from Alg and CMC) not only promotes the cross-linking reaction, but also transiently controls transmembrane ion diffusion [6,47], so nutrient release can be more flexibly controlled by compound coating materials. The cross-linking was verified by the new bonds with the absorption peak at 1606~1612 cm^{-1} in the FTIR spectra (Figure 9). However, considering the mechanical properties results (Table 3), too weak or too strong bonds resulted in unsatisfactory hardness

and springiness. It is reported that a higher concentration of Ca^{2+} leads to thicker coatings and higher stability [42], but lower swelling capacity [7]. Therefore, 10 mg g^{-1} was chosen in this study to balance this dilemma, in accordance with the opinion of de Matos et al. [5].

Ramos-Campos et al. [2] reported that high concentrations of Alg accelerate the release speed, while the effect of starch concentration was opposite. However, the results of Figure 5b did not completely support this opinion: the OSR of 30 mg g^{-1}-Alg treatment was slower than that of 20 mg g^{-1} treatment. In any case, since the *Eh* values of the 10 mg g^{-1}-Alg treatment were lower than those of the 20 mg g^{-1}- and 30 mg g^{-1}-Alg treatments, its HESD was shorter than those of these two treatments, and the granules of the 10 mg g^{-1}-Alg treatment were too soft to maintain their shape (Figures 4e,f and S6), it can be summarized that 20~30 mg g^{-1} was the satisfactory Alg concentration range for release control in this study.

Chiaregato et al. [43] suggested that the interaction between polymers and electrolyte media produces a denser and finer structure that delays release when the mass ratio of Chi and Alg was 1:1, but the material hydrophobicity increases with increasing Chi proportion. The Chi/Alg 20 mg g^{-1} Chi treatment in the single-factor assay just matched the 1:1 ratio, and it exhibited a stable and sustainable OSR curve (Figure 5e), which supported the above opinion.

Poor shape stability due to fertilizer-structure defects with high UP contents (Figures 2 and S2) might cause the granules to crumble after they were pressed, and the cavities in the granules decreased their densities, which made them float in the water layer rather than sink into paddy soil. Thus, oxidative substances and nutrients were released into the surface water and subsequently ran off. These disadvantages restricted the UP content range of fertilizer granules and their application. de Matos et al. [5] indicated that n-SiO_2, an environmentally friendly filler with small diameter, dominates porosity, hydrophobicity, and surface area of compound material: For instance, coated fertilizer with 5% (i.e., 50 mg g^{-1}) n-SiO_2 can maintain structural stability of internal space with sufficient porosity even with a 70-fold extension of surface area. Increasing n-SiO_2 content promotes water penetration and nutrient release when n-SiO_2 content is lower than the threshold value, while water and nutrient adsorption are enhanced if n-SiO_2 content exceeds the threshold. In any case, the corresponding threshold value of n-SiO_2 content in this study was 30 mg g^{-1} rather than 50 mg g^{-1} reported by de Matos et al. [5] (Figure 5c). The phenomenon that OSR in the treatments without n-SiO_2 was slower than in the treatments with n-SiO_2, except for the 30 mg g^{-1} n-SiO_2 treatment (Figure 5c), might be explained by the quasi-macroscopic structure of fertilizer granules (Figure 3): The addition of n-SiO_2 not only increased small-size pores but also eliminated larger-size pores inside granules induced by UP hydrolysis, so that more water and UP solution inside granules were retained by capillaries inside granules. Apart from optimizing structure (Figures 3, 4 and S4), the remarkable contribution of n-SiO_2 to alleviating the density decline caused by UP hydrolysis (Figure 7) might also be attributed to the higher density of n-SiO_2 itself. Moreover, the function of n-SiO_2 and CMC in hardness and springiness enhancement of coating material and fertilizer granules in this study (Table 3) has seldom been reported in previous literature, and their underlying mechanism is worthy of further investigation.

Fertilizer granules containing more UP seem to meet the purpose of this study. However, since the formula containing a low concentration of urea and Alg with a high cross-linking degree can also achieve a more efficient controlled-release structure [43], and considering the potential structure defect due to small pores inside fertilizer granules with high UP content (Figures 1 and S3), it was appropriate to set the UP content between 100 and 200 mg g^{-1} in this assay, and 150 mg g^{-1} was selected as the optimal content. The phenomenon that fewer visible UP crystals appeared in the 200 mg g^{-1} UP treatment

(Figure S3) seemed to be abnormal but was also explainable: the free water in Solution A dissolved UP rather than being retained by the Alg matrix after it was attracted by the high osmotic pressure from UP crystals with regionally high concentration. Similarly, a probable reason for the result of Figure S7b was that the free water in Solution B of the treatment that dissolved Alg and Chi first was less than that dissolved UP first; consequently, the corresponding UP hydrolysis speed was slower, and the oxygen loss during preparation was less in the latter one, so that its HESD was longer. On the other hand, since the water affinity of inorganic salt mixtures is generally stronger than organic polymers, coating materials are easily dehydrated by core inorganic fertilizers [64]; thus, the mechanical, physicochemical, and nutrient-release properties of bio-macromolecular materials are weakened. For instance, Llive et al. [6] found that increasing the urea proportion increases the diameter but decreases the density of fertilizer granules, while KH_2PO_4 leads to the opposite effect. Similarly, UP in this study amplified the density decline due to the combined effects of both urea and O_2 from UP hydrolysis (Figure 7).

Since there were Alg and Na_2SeO_4 in Solution A together, they reacted with $CaCl_2$ in Solution B simultaneously; thus, not only CaAlg but also $CaSeO_4$ formed in the final product, the latter one is regarded as a slow-release Se fertilizer due to its low solubility [18]. It was a pity that $CaSeO_4$ was not detected by XRD (Figure S9); in any case, the improvement in mechanical properties of the treatments with Na_2SeO_4 provided indirect evidence (Table 3). The peak shift of the carboxyl group (from 1427 cm^{-1} to 1422 cm^{-1} at maximum) in FTIR analysis (Figure 9) inferred that SeO_4^{2-} probably participated in the formation of new bonds rather than existing in free status, which agreed with the report of Ma et al. [65] that mesoporous silica nanoparticles loaded with Na_2SeO_4 modify Alg hydrogel and alleviate its controlled-release properties. However, since the contents of Na_2SeO_4 were low, the new bonds from $CaSeO_4$ were masked by the adjacent peaks of SiO_2 (Figure 9b,c). It should be noted that the peak at 820 cm^{-1} in Control 2 treatment might not be from SiO_2 but rather CO_3^{2-}, the product of UP hydrolysis (Figure 9b). Moreover, CaAlg and CMC are satisfactory release controllers for Se oxyanions by chelating and electrostatic binding from -OH and -COOH groups [10], as well as specific absorption [24], which remain when Se enters soils with coating material fragments simultaneously. Therefore, the controlled-release mechanism of the coating material in this study is both physical and chemical.

4.3. Oxidative Substance Release

The nutrient-release process of hydrogel CRF can be divided into two stages: (1) the hydrogel absorbs water and then swells; and (2) nutrients dissolve, permeate, and diffuse following the interface diffusion mechanism of water-soluble nutrients: water contacts the fertilizer granule surface, and then saturated water vapor enters the granules and dissolves the core fertilizer [46]. This process is driven by the solution osmotic pressure difference between inside and outside of granules, so it can be inferred that ambient humidity affects release speed [66]. According to the requirements of the European Union Standard for S/CRF (EN 13266) [67], it is acceptable that nutrient release of S/CRF follows the pattern of "fast–slow". Arafa et al. [1] indicated that urea coated by Alg–Chi compound material exhibited a fast-slow-equilibrium release pattern in deionized water since urea located on the granule coating surface or edges with loose binding can be quickly released after contacting with water [5], while the urea in other locations is released until water slowly permeates into the coating material matrix or the coating material is degraded. The results of single-factor assays (Figure 5) coincided with this pattern. On the other hand, the *Eh* drop at the beginning of the water-extraction assay and soil cultivation assays (Figure 8) might have resulted from the UP on the granule surface having lost oxidizability due to hydrolysis. Thus, the oxidative substances inside granules were blocked, and the *Eh* remained at a

low level until the surface Alg–Chi compound decomposed, which conversely consumed dissolved oxygen in extraction/soil solution. Moreover, osmotic pressure theory is also applicable for explaining this phenomenon [43]. However, there are other release models of CRF: Urea coated by papaya starch modified with polyvinylethanol is released following a pattern of "slow-constant speed-decay" [68]. The corresponding mechanism is that water permeating into the granule matrix initially forms a solution with high viscosity, which retards further water permeation and leads to slow release at first; the release speed then increases later as the solution becomes diluted in the second stage [43]. Nutrient-release burst occurs when the coating cracks due to aging or high osmotic pressure [69], which probably corresponds to the *Eh* dropping after slightly rising on the 15th day or later. In any case, the structure reinforced by n-SiO_2 and CMC delayed the third stage to the 30th day or later (Figures 5 and S7).

Since oxidative substances, rather than N nutrient in UP, were focused on in this study, the N release was not investigated, but *Eh* was measured instead. It should be noted that *Eh* is an index obtained from non-destructive measurement, which is suitable for screening many formulas in this study. However, since it is an intensive rather than extensive parameter, it cannot precisely describe and evaluate the number of oxidative substances released. On the other hand, determining residual UP can fulfill this target precisely, but it is not feasible currently because we failed to establish an UP content determination protocol that can exclude interference from Alg and Chi—notably, it cannot be regarded as certain that the release of oxidative substances and N nutrient from UP in S/CRF was synchronous when evidence is deficient. Therefore, it is inappropriate to assess OSR according to N release. Alternatively, another controlled-release component, Se, was measured in the soil assay in this study.

Moreover, the highest value of extraction solution *Eh* is restricted by redox equilibrium between H_2O_2 and O_2 as well as by the O_2 dissolution equilibrium at the water-air interface. Therefore, the treatments with similar highest *Eh* values (Figures 5 and 8) do not always indicate similar OSR properties since the potential *Eh*-elevating ability of some treatments may be leveled by the above equilibrium. However, the *Eh* upper limit in soil is significantly lower than in deionized water since more reductive substances act as restricting factors that complicate the redox equilibrium. Moreover, since soil microorganisms can degrade CaAlg and Chi, the crack speed of fertilizer granules in soil is possibly faster than in deionized water; consequently, the release duration of S/CRF in soil will be overestimated according to the deionized water assay. The *Eh* values in the soil assay were even lower than in free deionized water, and there was not a typical monotonic decrease but rather *Eh* fluctuation in the corresponding curves when oxidative substances were exhausted in soil (Figure 8).

4.4. Se Forms in Soil

Chemical forms in soil, the major nutrient reservoir, are an essential factor for plant micronutrient uptake [23,24,31], which depends on rhizosphere conditions, especially pH and *Eh* [32]. Since the UP concentration was 10,000 times that of Se, Se nutrient could not effectively influence *Eh* but was passively influenced by *Eh*; thus, the dominant valence of Se inside fertilizer granules was hexavalent regardless of its original valence. Both selenites and selenates are common Se fertilizers, and it seems that selenite is the default choice for paddy soils since little of the fertilized selenate can exist stably in soil with low *Eh*; rather, it transforms to selenite, elemental selenium, or selenide, and then it is immobilized under reductive conditions (Figure 10b–d). Also, selenite is the intermediate of selenate reduction inside plants [14,21,27]. However, selenate is beneficial for Se accumulation in shoots rather than roots of rice, which is similar for terrestrial plants [9,21,25,26,39]. In addition, the mobility of selenate is greater than selenite in soil [70,71] since positive sites in acidic soils

have high affinity for $HSeO_3^-$ species to form binuclear surface complexes [16], although this property is sometimes regarded as proof of selenite safety. Moreover, Sharma et al. [72] reported that Se^{VI} is not significantly adsorbed over the entire pH range when its concentration is lower than 30 mg L^{-1} in soil solution, while Se^{IV} can be retained at any concentration by all types of soils. Plants also attempt to absorb more selenate by actively secreting oxidative substances [71]; thus, supplying selenate to soil maintained under aerobic conditions is assumed to be the most effective strategy for elevating rice Se concentration [19,22]. Moreover, the Se^{VI} uptake rate of rice roots is slower than Se^{IV}; however, Se^{VI} is transported via the apoplastic pathway in plants, which is more efficient than the symplastic pathway for Se^{IV} transport [31,73]. So Na_2SeO_4 was used in this study because there was an oxidant (UP) in the fertilizer to maintain *Eh* at a relatively high level and overcome the difficulty of sustainable selenate supply in a reductive rhizosphere. Since both oxidative substances and selenate are released to the rhizosphere with mild intensity and lower Se toxicity risk, selenate could be absorbed in its original form by roots with a higher possibility. On the other hand, selenite consumes oxidants in the fertilizers, which shortens HESD in soil and is contrary to the aim of this study. Thus, it is unnecessary to select selenite for the above reasons. However, the *Eh* in bulk soil was significantly lower than the equilibrium electrode potential of Se^{VI}/Se^{IV} (493 mV under the condition of pH 5.5 and equal Se^{VI}/Se^{IV} concentration ratio) even when CRF continuously supplied oxidative substance (Figure 8b), so the dominant valence of released Se in actual bulk soil is tetravalent theoretically. However, the Se^{VI} contents were considerable (Figure 10b–d), which suggested that the soil was at redox disequilibrium status since Se^{VI} was also input continuously. In any case, selenite bonded by iron (hydr)oxides in soil (i.e., Se^{IV} fraction in Figure 10d) can still be regarded as a potential bioavailable Se resource [21] and has a similar effect on enhancing rice Se accumulation [19]. Thus, it is unnecessary to require a major proportion or even all the Se in the rhizosphere to be hexavalent (Figure 10).

Although its reaction rate constant is lower than that of other oxidants, including O_3, Mn^{VII}, and halogens [74], H_2O_2 has been proved to efficiently oxidize selenite and even elemental selenium to selenate and activate the soil organic Se pool under acidic conditions [20,75], as reported in our previous study that the cultivation medium can slightly acidify spontaneously during H_2O_2 oxidizing reductants [76]. The results of the soil cultivation assay in this study indicated that the oxidation effect of UP varied among different fractions at different stages: No treatment containing UP had a soluble Se^{VI} proportion that was consistently higher than the Se treatment throughout the whole assay, but those of Treatment II were higher than the Se treatment from the 40th to 80th day (Figure 10b). Similarly, the oxidizing effects of Control 4 and Treatment II at the 20th and 60th day, and those of Control 1, Control 4, and Se + UP treatment at the 80th day for Se_{exc} were significant (Figure 10c). Moreover, the Se^{VI} proportion of $Se_{Fe/Mn}$ in all treatments was lower than the initial value (Figure 10d). Considering the *Eh* variation, it could be inferred that UP mainly oxidizes Se_{sol}, and Se^{VI} in the exchangeable fraction might originate directly from the selenate released from fertilizer granules rather than Se that had been oxidized by UP in soil, while UP affected $Se_{Fe/Mn}$ little.

It is reported that flooding soil increases Se_{sol} concentration in the treatments without Se or with selenite, but decreases it markedly in the selenate treatment, although the results are opposite at the beginning of the assay. In addition, selenate is the main species in the selenate treatment, whereas selenite and organic Se are detected in the flooding soil solutions of the control and +selenite treatments [20]. The soil Se fraction results in this assay, in which selenate was supplied, partially supported this opinion: Hexavalence was the dominant Se valence for Se_{sol} and Se_{exc}, but flooding also decreased the Se^{VI} proportion of $Se_{Fe/Mn}$, which possessed a distinguishing proportion in total soil Se (Figure 10b,c,d,f). In

addition, it seemed abnormal that total soil Se contents of certain treatments at certain times decreased compared to previous corresponding values, e.g., Control 1, Se, and Se + UP treatments between the 40th and 60th day (Figure 10a). The probable explanation was that the mobility of exogenous selenate at a high concentration was high when it just entered paddy soil, which was more significant for the treatments with coated fertilizers. Thus, Se diffused to bulk soil far away from where fertilizer was applied, so that soil Se concentration was diluted in some respects; consequently, the Se concentration at the sampling sites decreased accordingly.

4.5. Application and Probable Solution for Further Modification

The OSR performance, i.e., soil *Eh* variation, of selected coating fertilizer products (Figure 8b) indicated that different *Eh* and Se variation patterns could be obtained with different coating formulas. Both the formulas of Control 1 and Treatment II could satisfy the demand for soil *Eh* elevation for a relatively long duration, so that they can be applied individually according to the needs: applying Control 1 and Treatment II formulas provided high *Eh* from the 20th to the 50th day and from the 30th to the 60th day after application, respectively. In any case, the "low-*Eh* gap" during the first 20 d needs to be paid attention to, which may cause nutrient loss due to low *Eh* during that period. Surprisingly, Control 4 formula, a formula without UP but containing Na_2SeO_4, also became the treatment with the highest soil bioavailable Se content at the 60th day, which meant that combining application of Treatment II, Control 1, and Control 4 formulas is necessary for consistent high bioavailable Se supply. However, it is feasible to fertilize only Control 1 formula 20 d or longer in advance before the maximum nutrition efficiency stage, from an economic perspective.

According to the performance in altering soil *Eh* and Se speciation (Figures 8 and 10) discussed above, we must acknowledge that the products in this study were far from satisfactory as Se fertilizers. However, they were satisfactory for elevating soil *Eh*; they did not efficiently alter the initial status that the Se fractions with low bioavailability, i.e., Se^{IV} of $Se_{Mn/Fe}$, Se_{ose}, and Se_{res} possessed a dominant proportion in soil Se speciation (Figure 10d–f), and even total soil Se content had reached the standard of "Se-rich" soil (Figure 10a). In addition, the transformation of Se_{ose} to other fractions was another remarkable effect of UP, but high *Eh* status from the 15th to 50th day could not hinder Se immobilization to the residual fraction (Figure 10e,f). In addition, it can be inferred that applying UP directly to soil is a double-edged sword since it increased soil adsorption for Se, especially Se^{IV} in $Se_{Fe/Mn}$, and decreased other proportions of Se simultaneously, even though it increased Se^{VI} in Se_{exc} at certain times (Figure 10c,d,f). According to the opinion of Rong et al. [23], the dominant fractions of considerable numbers of "Se-rich" soils are organic and residual Se rather than soluble and exchangeable ones, and the Se bioavailability of these soils is low even though they have high total Se content. Therefore, the results of Figure 10 were still explainable although it did not completely fulfill the target of this study, i.e., soil Se bioavailability enhancement, completely. The partial failure to elevate soil Se bioavailability in this study may be attributed to the incoordination of Se nutrient and oxidative substance release: A distinguishing feature of this incoordination was that the first 15 to 20 d during the assay, with low soil *Eh* (Figure 8b), was just the period of Control 1 and Treatment II supplying high bioavailable Se (Se_{sol}, Se_{exc} and Se^{VI} of $Se_{Fe/Mn}$) (Figure 10a–c). Due to a lack of sufficient oxidative conditions, the fate of considerable Se^{VI} released from fertilizer granules to soil during the first 20 d was immobilized as tetravalent $Se_{Fe/Mn}$ or Se_{res}, on the 40th day (Figure 10 d–f). The source of this problem was that the exploration and optimization of fertilizer formula mainly focused on OSR and physical properties, while the Se release properties received insufficient attention since we assumed that it was the same as, or at least similar to, that of OSR. In any case, this hypothesis was incorrect. Actually, Chi

was reported as an important component in superabsorbent for nutrients [77–79], which implies that considerable nutrients cannot be released until the coating material collapses if the adsorption is strong, so the nutrient retention properties of Alg–Chi–CMC coating material should be included in further study.

The above results also suggest that there are no generally optimal controlled-release formulas of coating material for all substances, so they need to be modified to achieve better release performance for specific substances. Apart from raising the UP content, revising the coating material formulas to optimize the release dynamics of Se and oxidative substances is an important solution for producing the S/CRFs with better performance in Se utilization efficiency enhancement. In this case, it is probably necessary to develop coating materials that provide different release patterns for Se nutrient and oxidative substances within a single formula, so that the oxidizing effect on the r Se nutrient can be more synergistic. Of course, more factors apart from components, e.g., cross-linking conditions, the internal structure of fertilizer granules, and combined application strategies of fertilizers with different release properties, need to be considered and explored. Moreover, field experiments with various types of soils need to be conducted under various climate conditions to examine their applicable range and corresponding features. Finally, it is worth noting that although UP and Na_2SeO_4 were embedded in fertilizer granules in this study, it was just an example to demonstrate the mechanical and release properties of the Alg–Chi–CMC–nSiO_2 compound coating material. This coating material can serve as a carrier for other substances whose controlled release can be tailored by altering embedded substances in the formula.

5. Conclusions

The addition of n-SiO_2 and CMC alleviated the oxidative substance release and improved the mechanical properties, especially hardness and density, of the CaAlg–Chi compound coating material, which was more significantly beneficial when UP existed. The optimal formula, 20~25 mg g^{-1} CaAlg, 15 mg g^{-1} Chi, 30 mg g^{-1} n-SiO_2, 10 mg g^{-1} CMC, 0.1 mg g^{-1} Na_2SeO_4 and 150 mg g^{-1} UP, performed most satisfactorily among the treatments, which had satisfactory properties in hardness, springiness and density. It elevated *Eh* by over 100 mV for at least 40 d compared to deionized water in the water-extraction assay and single Se treatment (i.e., coating fertilizer was not applied) in soil cultivation assays, respectively. Moreover, it increased the contents and proportions of soluble, exchangeable, and a part of Fe/Mn-binding Se, especially the hexavalent one, in soil, which was beneficial to Se accumulation in grains. Notably, selenate served not only as an encapsulated nutrient but also as a contributor to structure reinforcement. Although its performance in increasing soil bioavailable Se (Se_{sol}, Se_{exc} and a part of $Se_{Fe/Mn}$), especially the Se^{VI}, was not always significantly better than simply fertilizing with UP and Na_2SeO_4 as expected throughout the assay owing to the incoordination of Se and oxidative substance release, the release-control performance of this multi-component coating material has been verified by the OSR assay in this study. These coating material formulas provide a set of practical technical schemes for slow-release carriers for agricultural substances. However, they need to be modified in further studies to obtain formulas with more synergistic release performance for specific substances.

Supplementary Materials: The following supporting information can be downloaded at: https://www.mdpi.com/article/10.3390/polysaccharides7040126/s1. Figure S1: The surface and cross-section appearances of coated fertilizer granules prepared by different dissolution sequences; Figure S2: The cross-section scanning electronic micrographs of coated fertilizer granules prepared by different dissolution sequences; Figure S3: The cross-section scanning electronic micrographs of coated fertilizer granules with different UP contents; Figure S4: The effect of n-SiO_2 on coating fertilizer granule structure; Figure S5: The effect of UP on coating fertilizer granule structure when CMC and n-SiO_2 existed; Figure S6: The effect of Alg on coating fertilizer granule structure when CMC and n-SiO_2

existed; Figure S7: The water extraction solution *Eh* variation of fertilizer granules in tentative assay; Figure S8: The correlation coefficients between mechanical property parameters. The upper part indicated the correlation coefficients among blank and control treatments (the results of Table 3) while the lower part indicated the correlation coefficients among the treatments in the orthogonal design assay (the results of Figure 6); Figure S9: XRD patterns of (a) raw material, (b) blank and control treatments, as well as (c) treatments based on orthogonal design. Table S1, The components of treatments used in single factor assay; Table S2, The details of analysis of variance of the mechanical properties of fertilizer granules in orthogonal design assay (the results of Figure 6).

Author Contributions: Conceptualization, X.-J.Y. and H.S.; methodology, H.S. and X.-J.Y.; software, X.-J.Y.; validation, K.M. and Y.O.; formal analysis, Y.O. and K.M.; investigation, Y.O. and K.M.; resources, H.S. and X.-J.Y.; data curation, X.-J.Y.; writing—original draft preparation, X.-J.Y.; writing—review and editing, S.B. and H.S.; visualization, X.-J.Y.; supervision, S.B. and H.S.; project administration, X.-J.Y.; funding acquisition, S.B., H.S. and X.-J.Y. All authors have read and agreed to the published version of the manuscript.

Funding: This research was funded by the Guangdong Innovative Talent in General Institutions of Higher Education Program from the Department of Education of Guangdong Province, grant number 2022KQNCX009; and the Special Fund for Scientific Innovation Strategy-construction of High Level, Guangdong Academy of Agricultural Sciences from Guangdong Academy of Agricultural Sciences, grant number R2024YJ-YB3006.

Institutional Review Board Statement: Not applicable.

Data Availability Statement: Data are contained within the article or Supplementary Material. Further inquiries can be directed to the corresponding authors.

Acknowledgments: The authors express gratitude to Bingru Li, Shaomin Li, and Xiaolei Zhang of the College of Natural Resources and Environment, South China Agricultural University (SCAU) for their technical contribution in the preliminary exploration of this study; Xinwei Xie of the College of Materials and Energy, SCAU, for his assistance with X-ray diffraction analysis; and Weizhen Ou of the Analysis and Testing Center, SCAU, for her assistance with Fourier transform infrared spectrophotometry analysis.

Conflicts of Interest: The authors declare no conflicts of interest.

Abbreviations

The following abbreviations are used in this manuscript:

Alg	Alginate
CaAlg	Calcium alginate
Chi	Chitosan
CMC	Carboxymethylcellulose
Eh	Redox potential
FTIR	Fourier transform infrared spectrophotometry
HESD	High *Eh* sustaining duration
LDW	Level of deionized water
n-SiO_2	Silicon dioxide nanoparticle
OSR	Oxidative substance release
S/CRFs	Slow/controlled-release fertilizers
Se_{exc}	Exchangeable fraction of selenium
$Se_{Fe/Mn}$	Fe/Mn oxide-binding fraction of selenium
Se^{IV}	Tetravalent selenium content
Se_{ose}	Organic or sulfide binding/ elemental fraction of selenium
Se_{res}	Residual fraction of selenium
Se_{sol}	Water-soluble fraction of selenium
Se_t	Total selenium content of a certain soil fraction
Se^{VI}	Hexavalent selenium content
UP	Urea peroxide
XRD	X-ray diffraction

Appendix A. The Derivation of Equation (1) (The Equation for Density Calculation of Fertilizer Granules)

It is obvious that the relationship among the density of the fertilizer granule, ρ, its mass, $m_{\text{fertilizer}}$, and its volume, $V_{\text{fertilizer}}$, is:

$$\rho = \tag{A1}$$

according to the definition of density.

Then,

$$V_{\text{fertilizer}} = V_{\text{total}} - V_{\text{glycerol-1}} \tag{A2}$$

where V_{total} is the total volume of the pycnometer, i.e., V_0 in Equation (1); $V_{\text{glycerol-1}}$ is the volume of glycerol in the first filling (both fertilizer granules and glycerol were in the pycnometer). It should be noted that the viscosity coefficient of glycerol is 1000 times that of water and the duration that fertilizer granules contacted glycerol was within 15 min, so the possible process of glycerol penetrating the coating material and filling the internal pores of fertilizer granule samples can be omitted. Therefore, $V_{\text{fertilizer}}$ was the exact total volume of the fertilizer granule sample, including the solid phase and the internal pores.

Obviously,

$$V_{\text{glycerol-1}} = \tag{A3}$$

where $m_{\text{glycerol-1}}$ was the corresponding mass of glycerol in the pycnometer in the first filling, and

$$m_{\text{glycerol-1}} = m_2 - m_1 - m_0 \tag{A4}$$

Since only glycerol was in the pycnometer in the second filling, the density of glycerol, ρ_{glycerol}, can be calculated with the data in this filling:

$$\rho_{\text{glycerol}} = \tag{A5}$$

where $m_{\text{glycerol-2}}$ and $V_{\text{glycerol-2}}$ are the corresponding mass and volume of glycerol in the pycnometer in the second filling. Exactly,

$$m_{\text{glycerol-2}} = m_3 - m_0 \tag{A6}$$

$$V_{\text{glycerol-2}} = V_0 \tag{A7}$$

where the meanings of m_0, m_1, m_2, m_3 and V_0 are the same as those defined in Section 2.5.

Therefore, gathering Equations (A1)–(A7), ρ can be calculated with the data measured in the process described in Section 2.5

$$\begin{aligned}
\rho &= \frac{m_{\text{fertilizer}}}{V_{\text{total}} - \dfrac{m_{\text{glycerol-1}}}{\dfrac{m_{\text{glycerol-2}}}{V_{\text{glycerol-2}}}}} \\
&= \frac{m_1}{V_0 - \dfrac{m_2 - m_1 - m_0}{\dfrac{m_3 - m_0}{V_0}}} \\
&= \frac{m_1}{V_0 - \dfrac{(m_2 - m_1 - m_0)V_0}{m_3 - m_0}} \\
&= \frac{m_1(m_3 - m_0)}{(m_3 - m_0)V_0 - (m_2 - m_1 - m_0)V_0} \\
&= \frac{m_1(m_3 - m_0)}{(m_3 - m_2 + m_1)V_0}
\end{aligned} \tag{A8}$$

References

1. Arafa, E.G.; Sabaa, M.W.; Mohamed, R.R.; Kamel, E.M.; Elzanaty, A.M.; Mahmoud, A.M.; Abdel-Gawad, O.F. Eco-friendly and biodegradable sodium alginate/quaternized chitosan hydrogel for controlled release of urea and its antimicrobial activity. *Carbohydr. Polym.* **2022**, *291*, 119555. [CrossRef] [PubMed]
2. Ramos-Campos, E.V.; de Oliveira, J.L.; Fraceto, L.F.; Singh, B. Polysaccharides as safer release systems for agrochemicals. *Agron. Sustain. Dev.* **2015**, *35*, 47–66. [CrossRef]
3. Wu, L.; Liu, M. Preparation and characterization of cellulose acetate-coated compound fertilizer with controlled-release and water-retention. *Polym. Adv. Technol.* **2008**, *19*, 785–792. [CrossRef]
4. Naz, M.Y.; Sulaiman, S.A. Slow release coating remedy for nitrogen loss from conventional urea: A review. *J. Control. Release* **2016**, *225*, 109–120. [CrossRef] [PubMed]
5. de Matos, M.; Mattos, B.D.; Tardy, B.L.; Rojas, O.J.; Magalhães, W.L.E. Use of biogenic silica in porous alginate matrices for sustainable fertilization with tailored nutrient delivery. *ACS Sustain. Chem. Eng.* **2018**, *6*, 2716–2723. [CrossRef]
6. Llive, L.M.; Perullini, M.; Santagapita, P.R.; Schneider-Teixeira, A.; Deladino, L. Controlled release of fertilizers from Ca(II)-alginate matrix modified by yerba mate (*Ilex paraguariensis*) waste. *Eur. Polym. J.* **2020**, *138*, 109955. [CrossRef]
7. Shen, Y.; Wang, H.; Li, W.; Liu, Z.; Liu, Y.; Wei, H.; Li, J. Synthesis and characterization of double-network hydrogels based on sodium alginate and halloysite for slow release fertilizers. *Int. J. Biol. Macromol.* **2020**, *164*, 557–565. [CrossRef] [PubMed]
8. Zeng, X.; Han, B.; Xu, F.; Huang, J.; Cai, H.; Shi, L. Effects of modified fertilization technology on the grain yield and nitrogen use efficiency of midseason rice. *Field Crops Res.* **2012**, *137*, 203–212. [CrossRef]
9. D'Amato, R.; Regni, L.; Falcinelli, B.; Mattioli, S.; Benincasa, P.; Dal Bosco, A.; Pacheco, P.; Proietti, P.; Troni, E.; Santi, C.; et al. Current knowledge on selenium biofortification to improve the nutraceutical profile of food: A comprehensive review. *J. Agric. Food Chem.* **2020**, *68*, 4075–4097. [CrossRef] [PubMed]
10. Dev, S.; Khamkhash, A.; Ghosh, T.; Aggarwal, S. Adsorptive removal of Se(IV) by citrus peels: Effect of adsorbent entrapment in calcium alginate beads. *ACS Omega* **2020**, *5*, 17215–17222. [CrossRef] [PubMed]
11. El-Ramady, H.; Abdalla, N.; Taha, H.S.; Alshaal, T.; El-Henawy, A.; Faizy, S.E.D.A.; Shams, M.S.; Youssef, S.M.; Shalaby, T.; Bayoumi, Y.; et al. Selenium and nano-selenium in plant nutrition. *Environ. Chem. Lett.* **2016**, *14*, 123–147. [CrossRef]
12. Huang, G.; Ding, C.; Yu, X.; Yang, Z.; Zhang, T.; Wang, X. Characteristics of time-dependent selenium biofortification of rice (*Oryza sativa* L.). *J. Agric. Food Chem.* **2018**, *66*, 12490–12497. [CrossRef] [PubMed]
13. Jalalizand, F.; Goli, M. Optimization of microencapsulation of selenium with gum Arabian/Persian mixtures by solvent evaporation method using response surface methodology (RSM): Soybean oil fortification and oxidation indices. *J. Food Meas. Charact.* **2021**, *15*, 495–507. [CrossRef]
14. Li, Y.Y.; Yu, S.H.; Zhou, X.B. Effects of phosphorus on absorption and transport of selenium in rice seedlings. *Environ. Sci. Pollut. Res. Int.* **2019**, *26*, 13755–13761. [CrossRef] [PubMed]
15. Raina, M.; Sharma, A.; Nazir, M.; Kumari, P.; Rustagi, A.; Hami, A.; Bhau, B.S.; Zargar, S.M.; Kumar, D. Exploring the new dimensions of selenium research to understand the underlying mechanism of its uptake, translocation, and accumulation. *Physiol. Plant* **2020**, *171*, 882–895. [CrossRef] [PubMed]
16. Fan, J.; Zeng, Y.; Sun, J. The transformation and migration of selenium in soil under different Eh conditions. *J. Soils Sediments* **2018**, *18*, 2935–2947. [CrossRef]
17. Fang, Y.; Catron, B.; Zhang, Y.; Zhao, L.; Caruso, J.A.; Hu, Q. Distribution and in vitro availability of selenium in selenium-containing storage protein from selenium-enriched rice utilizing optimized extraction. *J. Agric. Food Chem.* **2010**, *58*, 9731–9738. [CrossRef] [PubMed]
18. Huang, P.; Yang, W.; Li, Q.; Liao, Q.; Si, M.; Shi, M.; Yang, Z. A novel slow-release selenium approach for cadmium reduction and selenium enrichment in rice (*Oryza sativa* L.). *Chemosphere* **2023**, *342*, 140183. [CrossRef] [PubMed]
19. Huang, Q.; Yu, Y.; Wang, Q.; Luo, Z.; Jiang, R.; Li, H. Uptake kinetics and translocation of selenite and selenate as affected by iron plaque on root surfaces of rice seedlings. *Planta* **2015**, *241*, 907–916. [CrossRef] [PubMed]
20. Li, H.; Lombi, E.; Stroud, J.L.; McGrath, S.P.; Zhao, F. Selenium speciation in soil and rice: Influence of water management and Se fertilization. *J. Agric. Food Chem.* **2010**, *58*, 11837–11843. [CrossRef] [PubMed]
21. Liu, X.; Zhao, Z.; Hu, C.; Zhao, X.; Guo, Z. Effect of sulphate on selenium uptake and translocation in rape (*Brassica napus* L.) supplied with selenate or selenite. *Plant Soil* **2016**, *399*, 295–304. [CrossRef]
22. Premarathna, L.; McLaughlin, M.J.; Kirby, J.K.; Hettiarachchi, G.M.; Stacey, S.; Chittleborough, D.J. Selenate-enriched urea granules are a highly effective fertilizer for selenium biofortification of paddy rice grain. *J. Agric. Food Chem.* **2012**, *60*, 6037–6044. [CrossRef] [PubMed]
23. Rong, Q.; Chen, J.; Zhang, Y.; Tan, Z.; Wang, W.; Sun, C.; Guo, X.; Zhou, C.; Cai, H.; Zhao, X. The interaction between selenium and other elements in soil and rice roots shaped by straw and straw biochar regulated the enrichment of selenium in rice grain. *Front. Plant Sci.* **2024**, *15*, 1387460. [CrossRef] [PubMed]

24. Pezzarossa, B.; Petruzzelli, G.; Petacco, F.; Malorgio, F.; Ferri, T. Absorption of selenium by *Lactuca sativa* as affected by carboxymethylcellulose. *Chemosphere* **2007**, *67*, 322–329. [CrossRef] [PubMed]
25. Ali, F.; Peng, Q.; Wang, D.; Cui, Z.; Huang, J.; Fu, D.; Liang, D. Effects of selenite and selenate application on distribution and transformation of selenium fractions in soil and its bioavailability for wheat (*Triticum aestivum* L.). *Environ. Sci. Pollut. Res. Int.* **2017**, *24*, 8315–8325. [CrossRef] [PubMed]
26. de Oliveira, A.P.; Nomura, C.S.; Naozuka, J. Evaluation of selenium enrichment of adzuki bean (*Vigna angularis*) sprouts: Translocation, bioaccessibility and Se-protein speciation. *Microchem. J.* **2017**, *134*, 19–26. [CrossRef]
27. Boersig, N.; Scheinost, A.C.; Shaw, S.; Schild, D.; Neumann, T. Retention and multiphase transformation of selenium oxyanions during the formation of magnetite via iron (II) hydroxide and green rust. *Dalton Trans.* **2018**, *47*, 11002–11015. [CrossRef] [PubMed]
28. Hermosillo-Cereceres, M.; Sánchez, E.; Muñoz-Márquez, E.; Guevara-Aguilar, A.; García-Bañuelos, M.; Ojeda-Barrios, D. Impact of selenium fertilization on the activity of detoxifying enzymes of H_2O_2. *Phyton* **2014**, *83*, 347–352. [CrossRef]
29. Zhu, Y.; Pilon-Smits, E.A.H.; Zhao, F.; Williams, P.N.; Meharg, A.A. Selenium in higher plants: Understanding mechanisms for biofortification and phytoremediation. *Trends Plant Sci.* **2009**, *14*, 436–442. [CrossRef] [PubMed]
30. Yin, H.; Qi, Z.; Li, M.; Ahammed, G.J.; Chu, X.; Zhou, J. Selenium forms and methods of application differentially modulate plant growth, photosynthesis, stress tolerance, selenium content and speciation in *Oryza sativa* L. *Ecotoxicol. Environ. Saf.* **2019**, *169*, 911–917. [CrossRef] [PubMed]
31. Lyubenova, L.; Sabodash, X.; Schroeder, P.; Michalke, B. Selenium species in the roots and shoots of chickpea plants treated with different concentrations of sodium selenite. *Environ. Sci. Pollut. Res. Int.* **2015**, *22*, 16978–16986. [CrossRef] [PubMed]
32. Premarathna, H.L.; McLaughlin, M.J.; Kirby, J.K.; Hettiarachchi, G.M.; Beak, D.; Stacey, S.; Chittleborough, D.J. Potential availability of fertilizer selenium in field capacity and submerged soils. *Soil Sci. Soc. Am. J.* **2010**, *74*, 1589–1596. [CrossRef]
33. Wang, D.; Zhou, F.; Yang, W.; Peng, Q.; Man, N.; Liang, D. Selenate redistribution during aging in different Chinese soils and the dominant influential factors. *Chemosphere* **2017**, *182*, 284–292. [CrossRef] [PubMed]
34. Lyu, L.; Wang, H.; Liu, R.; Xing, W.; Li, J.; Man, Y.B.; Wu, F. Size-dependent transformation, uptake, and transportation of SeNPs in a wheat-soil system. *J. Hazard. Mater.* **2022**, *424*, 127323. [CrossRef] [PubMed]
35. Skrzypczak, D.; Gil, F.; Izydorczyk, G.; Mikula, K.; Gersz, A.; Hoppe, V.; Chojnacka, K.; Witek-Krowiak, A. Innovative bio-waste-based multilayer hydrogel fertilizers as a new solution for precision agriculture. *J. Environ. Manag.* **2022**, *321*, 116002. [CrossRef] [PubMed]
36. Kögel-Knabner, I.; Amelung, W.; Cao, Z.; Fiedler, S.; Frenzel, P.; Jahn, R.; Kalbitz, K.; Kölbl, A.; Schloter, M. Biogeochemistry of paddy soils. *Geoderma* **2010**, *157*, 1–14. [CrossRef]
37. Sasidharan, R.; Hartman, S.; Liu, Z.; Martopawiro, S.; Sajeev, N.; van Veen, H.; Yeung, E.; Voesenek, L.A.C.J. Signal dynamics and interactions during flooding stress. *Plant Physiol.* **2018**, *176*, 1106–1117. [CrossRef] [PubMed]
38. Yang, C.M.; Yang, L.Z.; Yang, Y.X.; Zhu, O.Y. Rice root growth and nutrient uptake as influenced by organic manure in continuously and alternately flooded paddy soils. *Agric. Water Manag.* **2004**, *70*, 67–81. [CrossRef]
39. Zhou, X.; Yang, J.; Kronzucker, H.J.; Shi, W. Selenium biofortification and interaction with other elements in plants: A review. *Front. Plant Sci.* **2020**, *11*, 586421. [CrossRef] [PubMed]
40. Sapkota, Y.; Duball, C.; Vaughan, K.; Rabenhorst, M.C.; Berkowitz, J.F. Indicator of Reduction in Soil (IRIS) devices: A review. *Sci. Total Environ.* **2022**, *852*, 158419. [CrossRef] [PubMed]
41. Teixeira, L.S.; Pimenta, T.M.; Brito, F.A.L.; Malheiros, R.S.P.; Arruda, R.S.; Araujo, W.L.; Ribeiro, D.M. Selenium uptake and grain nutritional quality are affected by nitrogen fertilization in rice (*Oryza sativa* L.). *Plant Cell Rep.* **2021**, *40*, 871–880. [CrossRef] [PubMed]
42. Kozieł, W.; Jaromin-Gleń, K.; Polakowski, C.; Walkiewicz, A.; Bulak, P. Effect of encapsulated and free-living cells of *Chlorella vulgaris* L. on nitrogen retention in soils. *Int. Agrophys.* **2019**, *33*, 127–136. [CrossRef] [PubMed]
43. Chiaregato, C.G.; França, D.; Messa, L.L.; Dos Santos Pereira, T.; Faez, R. A review of advances over 20 years on polysaccharide-based polymers applied as enhanced efficiency fertilizers. *Carbohydr. Polym.* **2022**, *279*, 119014. [CrossRef] [PubMed]
44. Elsherbiny, A.S.; Galal, A.; Ghoneem, K.M.; Salahuddin, N.A. Novel chitosan-based nanocomposites as ecofriendly pesticide carriers: Synthesis, root rot inhibition and growth management of tomato plants. *Carbohydr. Polym.* **2022**, *282*, 119111. [CrossRef] [PubMed]
45. Ates, B.; Koytepe, S.; Ulu, A.; Gurses, C.; Thakur, V.K. Chemistry, structures, and advanced applications of nanocomposites from biorenewable resources. *Chem. Rev.* **2020**, *120*, 9304–9362. [CrossRef] [PubMed]
46. Bortolin, A.; Aouada, F.A.; de Moura, M.R.; Ribeiro, C.; Longo, E.; Mattoso, L.H.C. Application of polysaccharide hydrogels in adsorption and controlled-extended release of fertilizers processes. *J. Appl. Polym. Sci.* **2012**, *123*, 2291–2298. [CrossRef]
47. Sharma, R.; Bajpai, J.; Bajpai, A.K.; Acharya, S.; Shrivastava, R.B.; Shukla, S.K. Designing slow water-releasing alginate nanoreserviors for sustained irrigation in scanty rainfall areas. *Carbohydr. Polym.* **2014**, *102*, 513–520. [CrossRef] [PubMed]

48. Feng, Q.; Chen, M.; Wu, P.; Zhang, X.; Wang, S.; Yu, Z.; Wang, B. Simultaneous reclaiming phosphate and ammonium from aqueous solutions by calcium alginate-biochar composite: Sorption performance and governing mechanisms. *Chem. Eng. J.* **2022**, *429*, 132166. [CrossRef]
49. Kheirabadi, N.R.; Tabrizi, N.S.; Sangpour, P. Removal of nitrate from water by alginate-derived carbon aerogel modified by protonated cross-linked chitosan. *J. Polym. Environ.* **2019**, *27*, 1642–1652. [CrossRef]
50. Jindor, N.J.; Agorku, E.S.; Adimado, A.A. Starch-grafted sodium alginate-modified clay composites as environmentally controlled-release materials for NPK fertilizer. *Appl. Environ. Soil. Sci.* **2023**, *2023*, 5133023. [CrossRef]
51. Chen, Y.; Xu, Y.; El Idrissi, A.; Long, T.; Liu, Y.; Lu, L. Eco-friendly alginate-urea-fluroxypyr hydrogel for sustainable agriculture: A comprehensive approach to integrated fertilizer delivery and weed control. *Int. J. Biol. Macromol.* **2025**, *310*, 143257. [CrossRef] [PubMed]
52. Araujo, J.M.; Fortes-Silva, R.; Pola, C.C.; Yamamoto, F.Y.; Gatlin, D.R.; Gomes, C.L. Delivery of selenium using chitosan nanoparticles: Synthesis, characterization, and antioxidant and growth effects in Nile tilapia (*Orechromis niloticus*). *PLoS ONE* **2021**, *16*, e251786. [CrossRef] [PubMed]
53. Luo, Y.; Zhang, B.; Cheng, W.; Wang, Q. Preparation, characterization and evaluation of selenite-loaded chitosan/TPP nanoparticles with or without zein coating. *Carbohydr. Polym.* **2010**, *82*, 942–951. [CrossRef]
54. Zhang, Y.; Wei, W.; Lv, P.; Wang, L.; Ma, G. Preparation and evaluation of alginate-chitosan microspheres for oral delivery of insulin. *Eur. J. Pharm. Biopharm.* **2011**, *77*, 11–19. [CrossRef] [PubMed]
55. Liu, M.; Li, J.; Ren, B.; Liu, Y.; Liu, Z.; Zhou, T.; Cheng, D. The water-retaining functional slow-release fertilizer modified by carboxymethyl chitosan. *Carbohydr. Polym.* **2024**, *328*, 121744. [CrossRef] [PubMed]
56. Kim, H.J.; Bae, J.H.; Eom, Y. Creating ultra-strong and recyclable green plastics from marine-sourced alginate-chitosan nanowhisker nanocomposites for controlled release urea fertilizer. *Carbohydr. Polym.* **2025**, *347*, 122745. [CrossRef] [PubMed]
57. Pang, L.; Gao, Z.; Feng, H.; Wang, S.; Wang, Q. Cellulose based materials for controlled release formulations of agrochemicals: A review of modifications and applications. *J. Control. Release* **2019**, *316*, 105–115. [CrossRef] [PubMed]
58. Wang, X.; Wang, J.; Song, S.; Rao, P.; Wang, R.; Liu, S. Preparation and properties of soil conditioner microspheres based on self-assembled potassium alginate and chitosan. *Int. J. Biol. Macromol.* **2020**, *147*, 877–889. [CrossRef] [PubMed]
59. Tan, X.; Dong, G.; Shi, Z.; Zhang, D.; Liu, D.; Wang, Y.; Li, J.; Wang, P.; Zhang, W. Preparation and characterization of double-coated slow-release urea fertilizer encapsulated with polymethylmethacrylate and sulfonated cellulose derivatives modified sodium alginate hydrogel. *Int. J. Biol. Macromol.* **2025**, *319*, 145572. [CrossRef] [PubMed]
60. Zhang, H.; Yang, H.; Shao, J.; Chen, Y.; Zhang, S.; Chen, H. Multifunctional carboxymethyl cellulose sodium encapsulated phosphorus-enriched biochar composites: Multistage adsorption of heavy metals and controllable release of soil fertilization. *Chem. Eng. J.* **2023**, *453*, 139809. [CrossRef]
61. Liu, X.; Zhao, Z.; Duan, B.; Hu, C.; Zhao, X.; Guo, Z. Effect of applied sulphur on the uptake by wheat of selenium applied as selenite. *Plant Soil* **2015**, *386*, 35–45. [CrossRef]
62. Perez-Bravo, J.J.; Francois, N.J. Low cost and eco-friendly polymeric matrix prepared by physical cross-linking as potential potassium nitrate release system. *J. Appl. Polym. Sci.* **2022**, *139*, 51705. [CrossRef]
63. Klivenko, A.; Orazzhanova, L.; Mussabayeva, B.; Yelemessova, G.; Kassymova, Z. Soil structuring using interpolyelectrolyte complexes of water-soluble polysaccharides. *Polym. Adv. Technol.* **2020**, *31*, 3292–3301. [CrossRef]
64. Chen, Y.; Chen, Y. Thermo and pH-responsive methylcellulose and hydroxypropyl methylcellulose hydrogels containing K_2SO_4 for water retention and a controlled-release water-soluble fertilizer. *Sci. Total Environ.* **2019**, *655*, 958–967. [CrossRef] [PubMed]
65. Ma, X.; Zhang, S.; Yang, Y.; Tong, Z.; Shen, T.; Yu, Z.; Xie, J.; Yao, Y.; Gao, B.; Li, Y.C.; et al. Development of multifunctional copper alginate and bio-polyurethane bilayer coated fertilizer: Controlled-release, selenium supply and antifungal. *Int. J. Biol. Macromol.* **2023**, *224*, 256–265. [CrossRef] [PubMed]
66. Wei, B.; Jiang, J.; Gao, C.; Zhang, L.; Zhan, Y.; Jiang, S.; Li, Y.; Sun, S.; Xie, J.; Fan, X. Revealing channel controlled nutrient release mechanism of bio-oil polymer coated controlled-release fertilizer. *Ind. Crops Prod.* **2021**, *173*, 114096. [CrossRef]
67. Wang, J.; Liu, S.; Qin, Y.; Chen, X.; Xing, R.; Yu, H.; Li, K.; Li, P. Preparation and characterization of controlled-release fertilizers coated with marine polysaccharide derivatives. *Chin. J. Oceanol. Limnol.* **2017**, *35*, 1086–1093. [CrossRef]
68. Azeem, B.; KuShaari, K.; Naqvi, M.; Keong, L.K.; Almesfer, M.K.; Al-Qodah, Z.; Naqvi, S.R.; Elboughdiri, N. Production and characterization of controlled release urea using biopolymer and geopolymer as coating materials. *Polymers* **2020**, *12*, 400. [CrossRef] [PubMed]
69. Zhao, C.; Tian, H.; Zhang, Q.; Liu, Z.; Zhang, M.; Wang, J. Preparation of urea-containing starch-castor oil superabsorbent polyurethane coated urea and investigation of controlled nitrogen release. *Carbohydr. Polym.* **2021**, *253*, 117240. [CrossRef] [PubMed]
70. Coppin, F.; Chabroullet, C.; Martin-Garin, A.; Balesdent, J.; Gaudet, J.P. Methodological approach to assess the effect of soil ageing on selenium behaviour: First results concerning mobility and solid fractionation of selenium. *Biol. Fertil. Soils* **2006**, *42*, 379–386. [CrossRef]

71. Linam, F.A.; Limmer, M.A.; Seyfferth, A.L. Contrasting roles of rice root iron plaque in retention and plant uptake of silicon, phosphorus, arsenic, and selenium in diverse paddy soils. *Plant Soil* **2024**, *502*, 397–415. [CrossRef]
72. Sharma, V.K.; McDonald, T.J.; Sohn, M.; Anquandah, G.A.K.; Pettine, M.; Zboril, R. Biogeochemistry of selenium. A review. *Environ. Chem. Lett.* **2015**, *13*, 49–58. [CrossRef]
73. Wang, Q.; Kong, L.; Huang, Q.; Li, H.; Wan, Y. Uptake and translocation mechanisms of different forms of organic selenium in rice (*Oryza sativa* L.). *Front. Plant Sci.* **2022**, *13*, 970480. [CrossRef] [PubMed]
74. Liu, S.; Salhi, E.; Huang, W.; Diao, K.; von Gunten, U. Kinetic and mechanistic aspects of selenite oxidation by chlorine, bromine, monochloramine, ozone, permanganate, and hydrogen peroxide. *Water Res.* **2019**, *164*, 114876. [CrossRef] [PubMed]
75. Paydary, P.; Schellenger, A.E.P.; Teli, M.; Jaisi, D.P.; Onnis-Hayden, A.; Larese-Casanova, P. Chemical oxidation of selenite to selenate: Evaluation of reactive oxygen species and O transfer pathways. *Chem. Geol.* **2021**, *575*, 120229. [CrossRef]
76. Yang, X.; Khan, Z.; Ma, K.; Ouyang, Y.; Zhang, X.; Shen, H. Stable buffer couple series for rhizosphere oxidant-reductant potential regulation suitable for rice hydroponic cultivation experiments. *Plant Soil* **2023**, *493*, 673–696. [CrossRef]
77. Cao, C.; Huo, T.; Liu, P.; Long, J.; Ma, Y.; Jahan, S.I.; Manjoro, T.T.; Dong, F. Montmorillonite-sodium alginate/chitosan beads: A green potential solution for phosphorus removal from wastewater and slow-release phosphorus fertilizer application. *Int. J. Biol. Macromol.* **2025**, *305*, 141276. [CrossRef] [PubMed]
78. Jan, M.; Shalla, A.H.; Majid, K. Next-generation fertilizers: A TiO_2-chitosan composite superabsorbent as a sustained release N-fertilizer. *Langmuir* **2025**, *41*, 6323–6334. [CrossRef] [PubMed]
79. Kenawy, E.; Elnaby, H.H.; Azaam, M.M. Synthesis of superabsorbent composite based on chitosan-g-poly(acrylamide)/attapulgite. *Polym. Bull.* **2024**, *81*, 3527–3543. [CrossRef]

Disclaimer/Publisher's Note: The statements, opinions and data contained in all publications are solely those of the individual author(s) and contributor(s) and not of MDPI and/or the editor(s). MDPI and/or the editor(s) disclaim responsibility for any injury to people or property resulting from any ideas, methods, instructions or products referred to in the content.